

# **Synthesis, morphology and luminescent properties of $\text{Ca}_3\text{Y}_2\text{WO}_9:\text{Dy}^{3+}$ phosphors for w-LED applications**

A PROJECT REPORT  
SUBMITTED IN PARTIAL FULFILLMENT OF THE REQUIREMENTS  
FOR THE AWARD OF THE DEGREE

of

**MASTER OF SCIENCE**

in

**PHYSICS**

Submitted by:  
**ANKITA KHAN**  
**23/MSCPHY/84**  
**BHABANA DAS**  
**23/MSCPHY/89**

Under the supervision of  
**Dr. A.S. Rao**  
**Professor**  
&  
**Dr. Shailesh Narain Sharma**  
**Emeritus Professor**

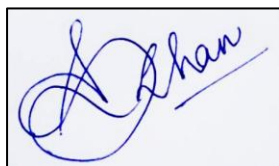


**DEPARTMENT OF APPLIED PHYSICS**  
**DELHI TECHNOLOGICAL UNIVERSITY**  
**(Formerly Delhi College of Engineering)**  
**Bawana Road, Delhi – 110042**  
**June, 2025**

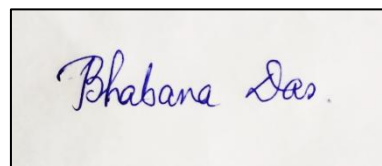
**DEPARTMENT OF APPLIED PHYSICS  
DELHI TECHNOLOGICAL UNIVERSITY  
(Formerly Delhi College of Engineering)  
Bawana Road, Delhi – 110042**

**CANDIDATES' DECLARATION**

We hereby declare that the project report titled “**Synthesis, morphology and luminescent properties of  $\text{Ca}_3\text{Y}_2\text{WO}_9:\text{Dy}^{3+}$  phosphors for w-LED applications,**” as a part of M.Sc. Physics Dissertation II, which is submitted by us to the Department of Applied Physics, Delhi Technological University, Delhi, in partial fulfillment of the requirement for the award of the degree of Master of Science in Physics, is original and not copied from any source without proper citation. The matter presented in this report has not been submitted for the award for any other course/degree of this or any other institute/university.



**Ankita Khan (23/MSCPHY/84)**



**Bhabana Das (23/MSCPHY/89)**

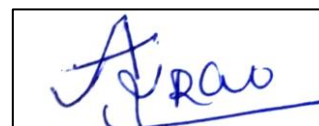
**Place: Delhi, Date: 9th June 2025**

**DEPARTMENT OF APPLIED PHYSICS  
DELHI TECHNOLOGICAL UNIVERSITY  
(Formerly Delhi College of Engineering)  
Bawana Road, Delhi – 110042**

**CERTIFICATE**

Certified that **ANKITA KHAN (23/MSCPHY/84)** and **BHABANA DAS (23/MSCPHY/89)** have carried out their research work presented in this project report titled “**Synthesis, morphology and luminescent properties of  $\text{Ca}_3\text{Y}_2\text{WO}_9:\text{Dy}^{3+}$  phosphors for w-LED applications**” for the award of the degree of Master of Science from Department of Applied Physics, Delhi Technological University, Delhi, under my supervision. The report embodies results of original work, and studies are carried out by the students themselves, and the contents of the report do not form the basis for the award of any other degree to the candidates or to anybody else from this or any other university/institution.

**Signatures:**

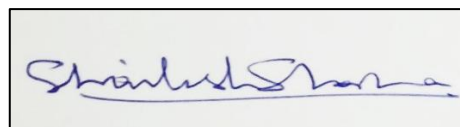


**Dr. A.S. Rao**

Professor

Department of Applied Physics  
Delhi Technological University, Delhi

**Place:** Delhi, **Date:** 9th June 2025



**Dr. Shailesh Narain Sharma**

Emeritus Professor

Department of Applied Physics  
Delhi Technological University, Delhi

**Place:** Delhi, **Date:** 9th June 2025

## ABSTRACT

Dysprosium ion-doped Calcium Yttrium Tungstate ( $\text{Ca}_3\text{Y}_2\text{WO}_9$ ) (CaYW) phosphors were synthesised via the solid-state reaction method. The undoped and doped phosphor samples were characterised by the x-ray diffraction (XRD) method. The diffraction peaks of the samples, sintered at  $1100^\circ\text{C}$ , closely resembled the Joint Committee on Powder Diffraction Standards (JCPDS) pattern with card number 00-038-0218, and the crystal system was found to be tetragonal. Scanning electron microscopy (SEM) was utilised to study the surface morphology of the samples. Diffuse reflectance spectroscopy (DRS) measured the optical band gap values.  $\text{CaYW}:\text{xDy}^{3+}$  phosphors, with different doping concentrations of  $\text{Dy}^{3+}$  ( $\text{x}=1, 3, 5, 7, 9$ , and  $11 \text{ mol}\%$ ), were synthesised, and their photoluminescence (PL) spectra were studied. The emission spectra revealed that the phosphors, when excited at  $352 \text{ nm}$ , showed intense emission at  $575 \text{ nm}$  (yellow light), corresponding to the transition  $^4\text{F}_{9/2} \rightarrow ^6\text{H}_{13/2}$ . Concentration quenching occurred after  $9 \text{ mol}\%$  of  $\text{Dy}^{3+}$  ions, and thus, the optimum phosphor sample is  $\text{CaYW}: 9\text{mol}\% \text{Dy}^{3+}$ . For all the samples of the phosphor, the Commission Internationale de l'éclairage (CIE) coordinates were evaluated, and they were found in the yellowish-white region. The coordinates for the optimum sample were  $(0.3654, 0.3972)$ . Fourier transform-infrared (FT-IR) spectra were analysed to identify the functional groups present in the samples. Thermogravimetric analysis (TGA) and temperature dependent-photoluminescence (TD-PL) analysis were also done to study the samples in a thermal context. In conclusion, the results of the current study demonstrate that the  $\text{Dy}^{3+}$  ions-doped CaYW phosphors may have the potential to be utilised in white light-emitting diodes (w-LEDs).

**Keywords:** phosphor, doping, luminescence, quenching, CIE chromaticity coordinates, w-LED.

## ACKNOWLEDGEMENTS

We would like to express our sincere gratitude to all those who have contributed to the successful completion of our dissertation. We are deeply grateful to **Ms. Bhawna**, Ph.D. Scholar, for her invaluable support in reviewing and editing the manuscript, as well as for her guidance in conceptualising the research and providing consistent supervision throughout the course of our work. We extend our heartfelt thanks to **Ms. Aarti**, Ph.D. Scholar, for her assistance and expert guidance with the experimental techniques involved in our study, along with her constant supervision. Our sincere appreciation goes to **Prof. Shailesh Narain Sharma** for his thorough review of our manuscript, as well as for his insightful validation and mentorship. We are equally thankful to **Prof. A.S. Rao** for his constructive feedback during the review process, his validation of our findings, and his unwavering academic supervision. Their collective guidance, encouragement, and expertise have been instrumental in shaping our research and bringing this dissertation to fruition.

## LIST OF RESEARCH WORK AND PUBLICATIONS

**Title of the Paper:** “Synthesis, morphology and luminescent properties of  $\text{Ca}_3\text{Y}_2\text{WO}_9\text{:Dy}^{3+}$  phosphors for w-LED applications”

**Authors:** Ankita Khan, Bhabana Das, Bhawna Rajpal, Aarti Yadav, Shailesh Narain Sharma, and A.S. Rao

**Name of the Conference:** 3rd International Conference on Advanced Functional Materials and Devices for sustainable development (AFMD-2025)

**Date and venue:** March 03-05, 2025, Atma Ram Sanatan Dharma College, Delhi University, Delhi

**Did you register for the conference?** Yes

**Status of paper (Accepted/Published/Communicated):** Communicated

**Journal:** Journal of Electronic Materials

**Date of paper communication:** 30th April, 2025

**Date of paper acceptance:** --

# **TABLE OF CONTENTS**

**Title page**

**Candidate's Declaration**

**Certificate**

**Abstract**

**Acknowledgements**

**List of Research Work and Publications**

**Contents**

**List of Figures**

**List of Tables**

**List of Abbreviations**

## **CHAPTER 1: INTRODUCTION**

1.1 Phosphor

1.2 Host material or matrix

1.2.1 Properties of host materials

1.2.2 Common host materials

1.2.3 Selection of host materials

1.3 Activator Ions

1.3.1 Role of Activator Ions in Luminescence

1.3.2 Factors to Consider When Selecting Activator Ions

1.3.3 Rare Earth Ions

1.4 Tungstate Phosphors

1.4.1 Properties of Tungstate Phosphors

1.5 Luminescence and its types

1.5.1 Understanding Photoluminescence through Jablonski diagram

## **CHAPTER 2: CHARACTERISATION TECHNIQUES**

2.1 X-ray diffraction method

2.2 Scanning electron microscopy

2.3 Diffuse reflectance spectroscopy

2.4 Photoluminescence spectroscopy

2.5 Commission Internationale de l'Éclairage coordinates and correlated colour temperature

2.6 Fourier transform infrared spectroscopy

2.7 Thermogravimetric and differential thermal analyses

2.8 Temperature-dependent photoluminescence spectroscopy

## **CHAPTER 3: EXPERIMENTAL PROCEDURE**

3.1 Synthesis of samples

3.2 Instrumentation

## **CHAPTER 4: RESULTS AND DISCUSSION**

4.1 X-ray diffraction (XRD) analysis

4.2 Scanning electron microscopic (SEM) analysis

4.3 Diffuse reflectance spectroscopic (DRS) analysis

4.4 Photoluminescence (PL) spectral analysis

4.5 Commission Internationale de l'Éclairage (CIE) coordinates and correlated colour temperature (CCT) analysis

4.6 Fourier transform-infrared spectroscopic (FT-IR) analysis

4.7 Thermogravimetric analysis (TGA) and differential thermal analysis (DTA)

4.8 Temperature dependent-photoluminescence (TD-PL) spectral analysis

## **CHAPTER 5: CONCLUSION**

## **REFERENCES**

## **PLAGIARISM REPORT**



**REGISTRATION AND PAYMENT PROOFS**

**CONFERENCE PARTICIPATION CERTIFICATES**

**CONFERENCE BOOK OF ABSTRACTS ACCEPTANCE PROOF**

**SUBMISSION TO JOURNAL OF ELECTRONIC MATERIALS**

**PROOF OF SCIE/SCOPUS INDEX**

## LIST OF FIGURES

**Figure 1.1.** Periodic table highlighting rare earth elements.

**Figure 1.2.** Jablonski diagram.

**Figure 2.1.** Bragg's law.

**Figure 2.2.** X-ray diffractometer.

**Figure 2.3.** A scanning electron microscope set-up.

**Figure 2.4.** Spectrophotometer for DRS.

**Figure 2.5.** Set-up for a spectrofluorometer.

**Figure 2.6.** A spectrometer for recording FT-IR spectrum.

**Figure 2.7.** Set-up for TGA.

**Figure 2.8.** Spectrometer to acquire TD-PL spectrum.

**Figure 3.1.** Precursor chemicals were ground for 1 hour, and they were stored in collection test-tubes.

**Figure 3.2.** Furnace.

**Figure 4.1.** X-ray diffraction (XRD) patterns for undoped CaYW and CaYW:9mol%Dy<sup>3+</sup>, along with the JCPDS pattern.

**Figure 4.2.** (a) SEM image for undoped CaYW, (b) SEM image for CaYW:9mol%Dy<sup>3+</sup>.

**Figure 4.3.** (a) Diffuse reflectance spectra for undoped and Dy-doped CaYW samples, (b) Tauc's plots for direct bandgap of undoped CaYW and doped CaYW phosphors.

**Figure 4.4** (a) Photoluminescence (PL) excitation spectra for all the Dy<sup>3+</sup>-doped CaYW phosphors, (b) emission spectra for the same samples.

**Figure 4.5.** Chromaticity diagram for CaYW:9mol%Dy<sup>3+</sup> phosphor sample.

**Figure 4.6.** Fourier transform-infrared (FT-IR) spectra for undoped and 9 mol% Dy<sup>3+</sup>-doped CaYW samples.

**Figure 4.7.** Thermogravimetric and differential curves for CaYW host matrix.

**Figure 4.8.** Temperature dependent-photoluminescence (TD-PL) spectra for CaYW:9mol%Dy<sup>3+</sup> phosphor at  $\lambda_{ex} = 352$  nm.

**Figure 4.9.** Linear plot of  $\ln\left[\left(\frac{I_0}{I_T}\right) - 1\right]$  vs  $1/K_B T$  to calculate the activation energy.

## LIST OF TABLES

**Table I.** Bandgap energy data for undoped CaYW and CaYW:xDy<sup>3+</sup> phosphors.

**Table II.** CIE coordinates for CaYW:xDy<sup>3+</sup> phosphors.

## **LIST OF ABBREVIATIONS**

LED: Light-emitting diode

w-LED: White Light Emitting Diode

RE: Rare Earth (Metals)

JCPDS: Joint Committee on Powder Diffraction Standards

XRD: X-ray Diffraction

SEM: Scanning Electron Microscopy

DRS: Diffuse Reflectance Spectroscopy

PL: Photoluminescence

CIE: Commission Internationale de l'Éclairage

CCT: Correlated Colour Temperature

IR: Infrared

UV: Ultraviolet

Vis: Visible

FT-IR: Fourier Transform Infrared

TGA: Thermogravimetric Analysis

DTA: Differential Thermal Analysis

TD-PL: Temperature Dependent Photoluminescence

# CHAPTER 1

## INTRODUCTION

# CHAPTER 1: INTRODUCTION

## 1.1 Phosphor

Solid substances known as phosphors release light when they come into contact with radiation, including ultraviolet, infrared, or electron beams. Phosphors come in a wide variety of forms, each with unique properties like colour emission and illumination duration. Since an alchemist named Vincentinus Casciarolo in Bologna, Italy, found a crystalline stone next to a volcano in the 17th century, the term "phosphors" has been in use. The stone was called "Bolognian stone" because, when exposed to sunlight, it gave off a crimson glow in the dark. The burning process created BaS, which is presently known as a host for phosphors, and the stone was subsequently determined to be barite ( $\text{BaSO}_4$ ).

The ability of phosphors to absorb energy and re-emit it as visible light or in other electromagnetic spectrum regions is one of their properties. Key characteristics include:

1. **Luminescence:** The release of light without significant heat production. This can occur in two main ways:
  - **Fluorescence:** The instantaneous emission of light upon activation.
  - **Phosphorescence:** Prolonged emission of light after the excitation source is removed.
2. **Decay Time:** How long does it take for the released light to fade after excitation? While fluorescence typically decays in nanoseconds, phosphorescence can last anywhere from seconds to hours.
3. **Emission Spectrum:** Phosphors emit light at specific wavelengths, which can be tuned by altering their composition.
4. **Efficiency:** The ability of a phosphor to convert absorbed energy into light.
5. **Durability:** Phosphors must be able to withstand prolonged excitation and environmental conditions without experiencing noticeable degradation [1–3].

## 1.2 Host material or matrix

In phosphors, host materials are the basic crystalline or amorphous substances that serve as a matrix for the addition of activator ions (dopants), which emit light when excited. Although these host materials don't emit light, they provide the electrical and structural conditions needed for the activators to function effectively.

The choice of host material has a significant effect on the stability, colour, and luminescence efficiency of the light that is released. Therefore, in some applications, optimising phosphor performance requires selecting the right host material [4,5].

### **1.2.1 Properties of host materials**

The host material needs to meet a number of criteria in order to function properly in a phosphor system:

1. **Crystal Structure:** A unique crystal lattice that has just the correct amount of symmetry to make activator ion incorporation easier. The lattice must allow for efficient energy transfer to the activators.
2. **Wide Bandgap:** The valence and conduction bands should have a large energy difference in order to prevent the host from absorbing the released light. The wide bandgap ensures transparency to the activator's emission wavelengths.
3. **Thermal Stability:** The material must remain stable at high temperatures during synthesis and use. This is particularly important for applications like LEDs and plasma screens.
4. **Low Phonon Energy:** When non-radiative loss is reduced, more energy can be released as light rather than dissipating as heat.
5. **Chemical Stability:** Resistance to environmental deterioration (such as moisture and oxidation) ensures long-term performance.
6. **Dopant Compatibility:** The activator ions (like transition-metal or rare-earth ions) should be supported by the host without causing noticeable energy losses or lattice distortion [2,4,5].

### **1.2.2 Common host materials**

1. **Oxides:** Two examples are zinc oxide (ZnO) and yttrium aluminium garnet (YAG). They are well known for their remarkable chemical and thermal resistance and are widely used in LEDs and display technologies.
2. **Sulphides:** Examples include zinc sulphide (ZnS) and calcium sulphide (CaS), which are commonly used in glow-in-the-dark materials and old CRT screens.
3. **Halides:** Examples include caesium iodide (CsI) and sodium iodide (NaI), which are utilised in scintillators for medical imaging and radiation detection.

4. Nitrides: Two examples are silicon nitride ( $\text{SiN}_4$ ) and aluminium nitride ( $\text{AlN}$ ). These materials are suitable for high-power LED applications and are renowned for their remarkable thermal stability.
5. Silicates: Because of their high brightness and stability, barium silicate ( $\text{BaSiO}_4$ ) and zirconium silicate ( $\text{ZrSiO}_4$ ) are commonly used in fluorescent lights.
6. Borates: Strontium borate ( $\text{SrB}_4\text{O}_7$ ) is one type that is utilised in optical applications to transform ultraviolet light into visible light.
7. Molybdates and Tungstates: Zinc molybdate ( $\text{ZnMoO}_4$ ) and calcium tungstate ( $\text{CaWO}_4$ ) are well known for their high luminescence efficiency, especially in X-ray screens.

### 1.2.3 Selection of host material

Selecting the ideal host material for a phosphor necessitates balancing several factors, depending on the intended use:

1. Application Requirements: Materials such as YAG are suggested for LEDs due to their thermal stability and compatibility with blue/UV light. Because of their long-lasting afterglow properties, sulphides like  $\text{ZnS}$  are chosen for glow-in-the-dark applications. Tungstates like  $\text{CaWO}_4$  are ideal for X-ray imaging due to their high density and capacity to absorb X-rays.
2. Energy Transfer Efficiency: The host material should efficiently transfer energy to the activator ions. Materials with low phonon energy, like oxides and nitrides, minimise energy loss.
3. Emission Wavelength: The host-activator combination determines the emission's colour. For example,  $\text{YAG:Ce}$  produces white or yellow light in LEDs, whereas  $\text{SrAlO}_4\text{:Eu}$  produces green light for glow-in-the-dark applications.
4. Stability: For outdoor applications, chemical stability against moisture and UV radiation is essential. Nitride and oxide are more stable than sulphides and halides [2,4,5].

### 1.3 Activator ions

Activator ions are the primary dopant components in phosphor materials that emit light. These ions are introduced into a host material to create energy states that allow efficient light absorption and emission. The brightness, colour, and overall efficiency of the phosphor are all



regulated by the activators. Selecting the appropriate activator ions is crucial when making phosphors for specific applications, such as LED lighting, displays, and medical imaging.

### **1.3.1 Role of activator ions in luminescence**

A phosphor's activator ions are excited to higher energy levels after absorbing energy from an outside source, such as electrons, X-rays, or ultraviolet light. When these ions return to their ground state, light (luminescence) is released.

1. Energy absorption: Involves excitation of the activator ion to a higher energy state.
2. Energy Conversion: Radiative recombination or relaxation releases photons with a specific wavelength.
3. Energy Losses (if any): Non-radiative processes, such as heat production. The wavelength (colour) of the light released depends on the activator ion's electrical makeup and its interactions with the host material [6].

### **1.3.2 Factors to consider when selecting activator ions**

Depending on the application and desired luminescence properties, a number of factors need to be considered when selecting an activator ion:

1. Emission Wavelength: The activator ion's electronic transitions dictate the colour released. For example, because it emits red light,  $\text{Eu}^{3+}$  is suitable for displays.  $\text{Ce}^{3+}$ , which emits blue to yellow light, is commonly used in white LEDs.
2. Energy Levels and Transition Mechanisms: The necessary emission wavelength should be aligned with the ground state and excited state energy gaps of the activator. Rare-earth ions (4f-4f transitions) generate sharper spectral lines, whereas transition metals (d-d transitions) offer broader emissions.
3. Host Material Compatibility: With minimal to no lattice distortion, the activator ion should mix well with the host lattice. For example,  $\text{Mn}^{2+}$  works well in ZnS-based hosts.  $\text{Ce}^{3+}$  mixes well with Yttrium Aluminium Garnet (YAG) hosts.
4. Luminescence Efficiency: Efficiency is determined by how well the activator absorbs excitation energy and re-emits it as light. Quantum efficiency and the reduction of non-radiative losses are important considerations.
5. Excitation Source: The energy source of the application must cause the activator to react. For example, LEDs can be excited by either blue or UV light using  $\text{Ce}^{3+}$ .  $\text{Eu}^{2+}$  is used in medical imaging to detect X-rays.

6. **Chemical and Thermal Stability:** The activator ion must remain stable under operating conditions, such as high temperatures in LEDs or exposure to moisture in outdoor applications.
7. **Activator Concentration:** It's important to have the right activator concentration. Too low concentrations cause weak emission, while too high concentrations cause concentration quenching, or energy losses caused by ion-ion interactions.
8. **Cost and Availability:** Rare-earth activators can be expensive because of supply chain constraints. Alternatives such as transition metal ions may be considered for applications where cost is an issue [7–9].

### 1.3.3 Rare earth ions

The development of phosphors has led to the widespread use of rare earth (RE) elements as luminous centres or activators in various host lattices. These components are employed despite their high cost because they can generate precise spectrum distributions, which makes them highly useful for commercial applications. The market for luminous materials doped with rare earth elements (RE) has been growing steadily due to their remarkable quantum efficiency, stability, and wide range of applications. Rare earth (RE) elements are a group of 17 elements that usually include the 15 lanthanides (ranging from La, which has atomic number 57, to Lu, which has atomic number 71), Sc, which has atomic number 21, and Y, which has atomic number 39. Although these elements are abundant in the Earth's crust, they are rarely found in concentrated, marketable forms. Each energy level of the ion has distinct luminous characteristics due to the partially occupied 4f orbitals of the lanthanides,  $\text{Ce}^{3+}$  to  $\text{Lu}^{3+}$ . Luminescent ions are commonly employed as dopants in a variety of host phosphor lattices. RE ions are essential to display technology due to their remarkable luminous characteristics, which are characterised by distinct peak emission bands. They are also necessary for radiation detection and solid-state material lighting. To be utilised in industrial settings, phosphors need to possess remarkable luminous efficiency, unparalleled chemical stability, temperature control, extended operational life, and environmentally friendly properties. The appropriate doping of rare earth (RE) elements to attain these properties has been one of the primary research topics. Narrow band emitting phosphors (such as  $\text{Sm}^{3+}$ ,  $\text{Tm}^{3+}$ ,  $\text{Er}^{3+}$ , and  $\text{Nd}^{3+}$ ) and broad band emission phosphors (such as  $\text{Eu}^{2+}$ ,  $\text{Tb}^{3+}$ ,  $\text{Gd}^{3+}$ ,  $\text{Yb}^{3+}$ ,  $\text{Dy}^{3+}$ , and  $\text{Ce}^{3+}$ ) are the two main categories of phosphors doped with rare earth elements based on their emission characteristics. The high sensitivity of the 5d-4f transitions in ions such as  $\text{Eu}^{2+}$  and  $\text{Ce}^{3+}$  to local structural changes results in the production of broad band emissions. Nonetheless, the

shielding effect keeps the neighbouring atom arrangement from having an effect on most 4f levels. As a result, they produce steady, consistent emission spectra with distinctive features. By varying the doping concentration and the targeted occupancy of rare earth (RE) ions at different crystallographic locations, the optical properties of the host materials can be precisely modified. The crystal field interaction, particularly with the 5d orbital, has a significant impact on the emission colour and excitation wavelength of 4f-5d transitions. For instance, the 5d excited state of the Ce<sup>3+</sup> ion is significantly influenced by the crystal structure, resulting in a discernible shift in the emission spectrum towards longer wavelengths. In conclusion, rare-earth ions are necessary for the creation of high-performance luminous materials, particularly those for use in solid-state lighting (SSL) and display technologies. Their distinctive electronic transitions and combinations offer a starting point for designing effective, durable, and adaptable lighting systems [2,4].

H	Rare Earth Elements																He	
Li	Be											B	C	N	O	F	Ne	
Na	Mg											Al	Si	P	S	Cl	Ar	
K	Ca	Sc	Ti	V	Cr	Mn	Fe	Co	Ni	Cu	Zn	Ga	Ge	As	Se	Br	Kr	
Rb	Sr	Y	Zr	Nb	Mo	Tc	Ru	Rh	Pd	Ag	Cd	In	Sn	Sb	Te	I	Xe	
Cs	Ba	*	Hf	Ta	W	Re	Os	Ir	Pt	Au	Hg	Tl	Pb	Bi	Po	At	Rn	
Fr	Ra	**	Rf	Db	Sg	Bh	Hs	Mt	Ds	Rg	Cn	Uut	Fl	Uup	Lv	Uus	Uuo	
		*	La	Ce	Pr	Nd	Pm	Sm	Eu	Gd	Tb	Dy	Ho	Er	Tm	Yb	Lu	
		**	Ac	Th	Pa	U	Np	Pu	Am	Cm	Bk	Cf	Es	Fm	Md	No	Lr	
			Light Rare Earth Element										Heavy Rare Earth Element					

**Figure 1.1.** Periodic table highlighting rare earth elements.

## 1.4 Tungstate phosphors

Tungstate molecules ( $\text{WO}_4^{2-}$ ) serve as the host for the luminescent compounds called tungstate phosphors. These phosphors are well known for their broad bandgap, high efficiency, and remarkable chemical and thermal durability. The tungstate ion, often coupled with rare-earth or transition-metal ions, contributes to a range of emission colours depending on the activator used.

### 1.4.1 Properties of tungstate phosphors

1. **High Luminescence Efficiency:** Tungstate materials have excellent ultraviolet (UV) absorption and efficiently convert absorbed energy into visible light.

2. **Thermal and Chemical Stability:** Tungstate compounds, like calcium tungstate ( $\text{CaWO}_4$ ) and zinc tungstate ( $\text{ZnWO}_4$ ), can withstand high temperatures and are not easily broken down by chemicals.
3. **Broad Bandgap:** Tungstate hosts' broad bandgap ( $\sim 4\text{--}5\text{ eV}$ ) makes them suitable for applications requiring UV or high-energy stimulation.
4. **Versatile Emission:** When doped with the appropriate activators, tungsten state phosphors can emit in the red, green, and blue regions of the visible spectrum.
5. **High Density:** Tungsten materials are ideal for applications requiring interaction with high-energy radiation, such as X-rays or gamma rays, due to their thickness.
6. **Long Decay Times:** Certain tungstate phosphors have long afterglow properties that make them useful for glow-in-the-dark or persistent luminescence imaging applications [2,10,11].

### **1.5 Luminescence and its types**

After the discovery of phosphors in the 17th century, every researcher started searching for new explanations for luminescence and its causes. Luminescence is the process by which a substance emits light without producing heat. The result of a substance absorbing incident energy and re-emitting it at a different wavelength is called luminescence. Numerous methods, such as heat, electricity, mechanical force, chemical reactions, and more, can be used to excite phosphorus. Many commonplace items, including lamps, televisions, and smartphone screens, exhibit luminescence.

Depending on the various excitation sources, the luminescence phenomena can be divided into several groups:

1. **Photoluminescence:** When electromagnetic radiation hits the surface of a phosphor, electrons are excited. It can be separated into two groups based on the technique: phosphorescence and fluorescence.
2. **Chemiluminescence:** A chemical reaction causes this kind of light emission. This reaction can happen without heat or external light because it is self-contained within the chemical system. The emission of light is mostly caused by an electronic transition that takes place within the molecules involved in the chemical process. The firefly is a well-known example of a live organism that exhibits chemiluminescence. The enzyme luciferase facilitates the chemical reaction between luciferin and oxygen, which releases light. In forensic investigations, a chemiluminescent material known as luminol is used to find blood at crime scenes.

3. Bioluminescence: Chemical reactions in living organisms produce this type of luminescence. It is found in many organisms, such as deep-sea fish, bacteria, fungi, and insects.
4. Thermoluminescence: This is the process by which certain materials produce light when heated after being exposed to ionising radiation. This method is frequently employed in dosimetry to quantify radiation exposure and in geology and archaeology for dating. The fundamental concept is that certain minerals and substances gradually store energy from ionising radiation, which is subsequently released as light when the material is heated.
5. Electroluminescence: This method produces luminescence by exposing the phosphor to an electric field. Similar to LEDs, electron-hole pair recombination is what produces the illumination. Free electron-induced luminescence is referred to as cathodoluminescence.
6. Radioluminescence: When certain materials are exposed to ionising radiation, they produce visible light. This process is different from thermoluminescence, which is the process by which a material that has been exposed to ionising radiation and heated produces light. Radioluminescence is the direct emission of light caused by interaction with ionising radiation.
7. Mechanoluminescence: Luminescence results from any mechanical influence on the phosphor.
8. Piezo-luminescence: This method, which happens when pressure is applied to a substance, is called piezo-luminescence [12].

### **1.5.1 Understanding photoluminescence through Jablonski diagram**

Photoluminescence is the process by which a substance absorbs photons, or packets of light energy, and then emits light. This phenomenon occurs when a material is exposed to a specific wavelength of light, resulting in the emission of a longer wavelength of light. Essentially, photon energy is absorbed by the material and released as light. The two primary forms of photoluminescence are fluorescence and phosphorescence. These are explained quite simply in the Jablonski diagram.

1. Phosphorescence is the process by which materials retain their ability to produce energy and shine even after the radiation source has been switched off. The brightness of this glow gradually fades over milliseconds to days. This phenomenon can happen when two excited states with different total spins exhibit similar energy levels. The ground state and one of the excited states are shown as a singlet ( $S=0$ ), while the next excited

state is shown as a triplet ( $S=1$ ). Spectroscopic transitions between singlet and triplet levels are forbidden by the rule  $\Delta S=0$ , but this is not true if the excited states are transferred kinetically, that is, by collision-induced radiationless transitions. A transfer between the two potential curves is only possible close to the cross-over point. The molecule can't go back to the excited singlet state once it enters the triplet state and begins to lose vibrational energy. As a result, it will eventually arrive at the triplet state's zero velocity level ( $\ddot{v}=0$ ). Although spectroscopic constraints technically forbid it, a transition from the current state to the ground state is feasible, albeit much more slowly than an electronic transition that is permitted. Phosphorescent materials can radiate for seconds, minutes, or even hours after absorbing energy. The phosphorescence spectrum typically consists of frequencies lower than those absorbed [12].

2. The process by which materials rapidly generate energy and cease to glow when the stimulating radiation is removed is known as fluorescence. The phenomenon can be explained by a figure that depicts the molecule in a highly vibrating state following electronic excitation. Any extra vibrational energy in this state can be released through intermolecular collisions. When vibrational energy is converted to kinetic energy, heat is created in the sample. "Radiationless" means that energy can move between different levels without emitting radiation. After transitioning to a lower vibrational state, the excited molecule emits radiation and settles back to its ground state. This released radiation is known as the fluorescence spectrum, and it typically has a lower frequency than the absorbed light. But under certain circumstances, it might happen more frequently. The time interval between the chemical's initial absorption and its return to its initial state is extremely short, measuring only  $10^{-8}$  seconds [12].

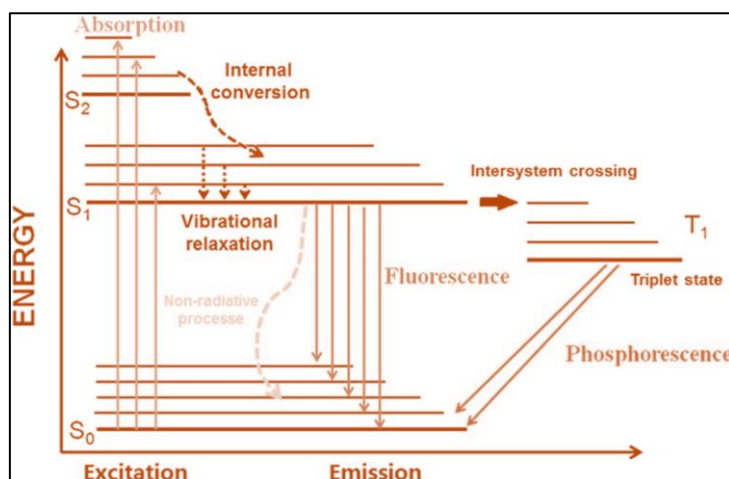


**Figure 1.2.** Jablonski diagram.

# **CHAPTER 2**

## **CHARACTERISATION TECHNIQUES**

## CHAPTER 2: CHARACTERISATION TECHNIQUES

### 2.1 X-Ray diffraction method

X-ray diffraction is a widely used technique to determine a material's crystal structure, phase purity, crystallite size, distance between crystal planes, lattice parameters, and stresses. This method was developed in 1912 by German physicist von Laue. The English physicists W.H. and W.L. Bragg were the first to successfully determine the crystal structures of different crystals using the XRD method.

The wavelength of the electromagnetic waves that comprise x-rays is approximately a few Angstroms (10-10 m). The German physicist Roentgen discovered it in 1895. The phenomenon of light diffraction is well known in optics. The way light is bent by an obstruction or an aperture is called diffraction. Diffraction occurs because the obstruction's corners act as secondary light sources and each wave they emit has a phase relation. Diffraction occurs when the width of the obstruction is less than or equal to the wavelength of the wave. X-rays can be diffracted from the crystal lattice because the inter-planar distances ( $d$ ) are comparable to the x-ray wavelength. The phase difference brought on by the atomic planes is given by the relation  $2d\sin\theta=n\lambda$ .

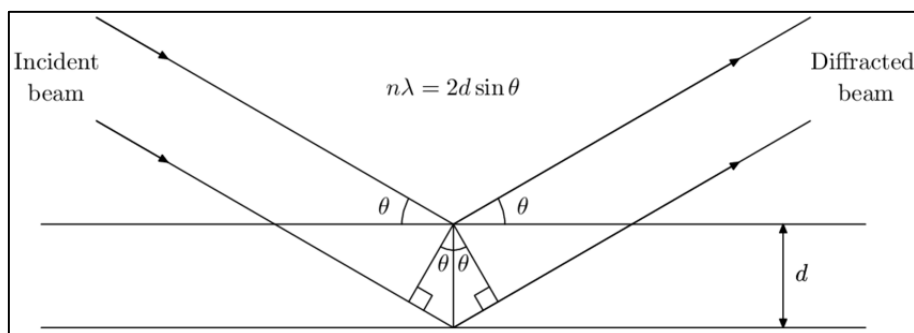


**Figure 2.1.** Bragg's law.

This equation is known as Bragg's law. In this case,  $d$  represents interplanar distance,  $\lambda$  the wavelength of the X-ray, and  $\theta$  Bragg's angle.

A detector, which can be stationary or mobile, picks up X-rays that have been diffracted in all directions by the sample. Depending on the geometry of the experiment, there are three types of XRD methods:

1. Laue's method
2. The method of rotating crystal
3. The Debye-Scherrer method, also known as the powder crystal method

The powder crystal method is frequently used to prepare this finely powdered sample. The strength of the diffracted beams at different diffraction angles ( $\theta$ ) is measured by the detector.



The intensity of the diffracted beam at different  $\theta$  positions is determined by the crystal structure and the alignment of the atomic planes. The obtained spectrum is then compared to the widely used databases that the Joint Committee on Powder Diffraction Standards (JCPDS) has made available. This spectrum is used to determine the crystal structure and other characteristics.



**Figure 2.2.** X-ray diffractometer.

## **2.2 Scanning electron microscopy**

Scanning electron microscopy (SEM), a powerful imaging technique, has advanced significantly in the fields of materials science, biology, and nanotechnology. The transmission electron microscope (TEM), developed in 1931 by Ernst Ruska and Max Knoll, began to change in the early 1900s. In 1935, Max Knoll conducted the first experiments involving the scanning of a focused electron beam across a specimen surface. But in 1942, Manfred von Ardenne constructed a more practical SEM. The technology reached maturity in 1965 when the Cambridge Instrument Company released the first commercial SEM. Since then, SEM has evolved to offer digital imaging capabilities, sophisticated detection systems, and resolution at the nanometre scale.

The theory behind SEM is based on how a high-energy electron beam interacts with the atoms in a sample. When the finely focused electron beam strikes the sample surface, it

produces a range of signals due to elastic and inelastic scattering processes. These include backscattered electrons (BSE), which are high-energy electrons reflected back from deeper within the sample and provide compositional contrast; characteristic X-rays, which are created by electronic transitions within the sample's atoms and are used for elemental analysis through Energy Dispersive X-ray Spectroscopy (EDS or EDX); and secondary electrons (SE), which are low-energy electrons ejected from the sample's surface atoms and are primarily used for detailed topographical imaging.

The operation of the SEM involves several key components. Electrons from an electron gun, which typically uses a tungsten filament, LaB<sub>6</sub> crystal, or a field emission source, are focused into a narrow beam by electromagnetic condenser lenses. This beam is rastered across the sample surface using scanning coils. A range of signals are produced as the electron beam interacts with the sample. To stop air molecules from scattering electrons, the sample is maintained in a vacuum chamber. Detectors collect these signals: SE for surface detail, BSE for composition, and X-rays for elemental information. Following processing, these signals appear as high-resolution images with contrast that matches signal strength.



**Figure 2.3.** A scanning electron microscope set-up.

### 2.3 Diffuse reflectance spectroscopy

Diffuse Reflectance Spectroscopy (DRS) is a non-destructive analytical technique that focusses on the optical properties of powders, rough surfaces, and opaque materials. It began in the early 20th century with improvements in reflectance measurement techniques, but it really took off in the mid-1900s when integrating spheres and UV-Vis spectrophotometers became more widely available. Over time, DRS has become increasingly important in fields such as material science, pharmacology, geology, and catalysis, particularly for studying chromophores, band gaps, and electronic transitions in solid materials.

The theoretical foundation of DRS is the interaction of incident light with a diffusely scattering surface. Unlike specular reflection, which occurs at a specific angle, diffuse reflection occurs when light enters a rough or particulate surface, undergoes multiple scattering events, and then departs in a variety of directions. During this process, some of the light is reflected back and some is absorbed by the substance. By measuring the intensity of this reflected light as a function of wavelength, the technique ascertains the optical absorption characteristics of the material.

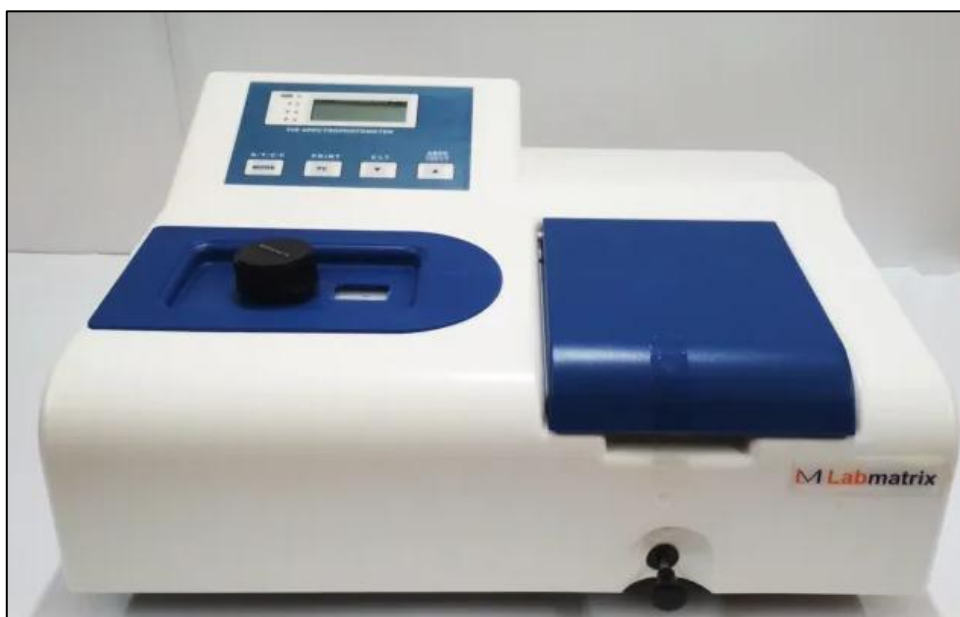


**Figure 2.4.** Spectrophotometer for DRS.

DRS involves exposing a powdered or matte solid sample to a UV, visible, or near-infrared light beam. The sample is typically placed inside an integrating sphere to collect the diffusely reflected light from all directions. The light is then directed onto a detector, which uses various wavelengths to measure its intensity. Since sample transparency is not required, the method is ideal for studying materials that are opaque or have high scattering qualities. The resulting spectrum shows electrical transitions, band gap energies, and information about the chemical

composition and molecular structure. DRS offers a rapid and minimally invasive method of material characterisation, and it is particularly helpful for samples that are insoluble or unstable in gearbox configurations.

## 2.4 Photoluminescence spectroscopy

Photoluminescence (PL) spectroscopy is a sensitive, non-destructive optical technique for investigating the electrical and optical properties of materials, especially semiconductors, insulators, and nanomaterials. Originating in the early study of luminous phenomena in the 19th century, the technique gained increasing scientific and technological significance with the introduction of solid-state physics and laser excitation sources in the mid-20th century. Nowadays, PL spectroscopy is frequently used in both industry and research for material characterisation, defect analysis, and band structure analysis.

The theoretical basis of PL spectroscopy is provided by the process of photoluminescence, in which a material absorbs photons and then re-emits them. When a sample is exposed to enough energy from light, usually visible or UV light, its electrons are excited from the valence band to the conduction band, leaving holes behind. As these electrons return to lower energy states, either directly to the valence band or through intermediate defect or impurity levels, photons are released. The energy (and thus wavelength) of this emitted light can be used to directly infer energy differences between electronic states, such as band gaps, impurity levels, and exciton dynamics. The position, intensity, and shape of the emission peaks reveal details about the material quality, carrier recombination processes, and crystalline defects.



**Figure 2.5.** Set-up for a spectrofluorometer.

In a typical PL spectroscopy setup, the sample is illuminated by a monochromatic light source, usually a laser, whose energy exceeds the material's band gap. The produced photoluminescence is collected using optical elements such as lenses or mirrors and transmitted

via a monochromator to a detector, usually a charge-coupled device (CCD) or a photomultiplier tube (PMT). Measurements can be performed in a cryogenic environment or at room temperature to resolve fine spectral characteristics. The recorded spectrum, which displays the intensity of light emitted as a function of wavelength or energy, can be analysed to determine band gap energies, identify impurities or defects, and assess quantum efficiency.

## **2.5 Commission Internationale de l'Éclairage coordinates and correlated colour temperature**

The Commission Internationale de l'Éclairage (CIE) coordinates and Correlated Colour Temperature (CCT), which are used to measure and objectively characterise the colour of light, are two fundamental concepts in colourimetry. These metrics are essential in fields like lighting design, display technology, photography, and material research where accurate colour representation and communication are crucial.

CIE coordinates originate from the CIE 1931 colour space, which was developed by the Commission Internationale de l'Éclairage to provide a mathematical model for human colour vision.

To describe the colour appearance of a light source, one uses the temperature (in kelvins, K) of a blackbody radiator that emits light of a similar hue. We call this Correlated Colour Temperature (CCT). Even though the majority of actual light sources don't produce true blackbody radiation, their colour can still be "correlated" with the closest point on the blackbody locus of the CIE chromaticity diagram. Warm light, such as that from incandescent bulbs, has a low CCT (about 2700–3000 K), appearing reddish or yellowish, while cool light, such as daylight or some LEDs, has a high CCT (over 5000 K), appearing bluish.

## **2.6 Fourier transform infrared spectroscopy**

Fourier Transform Infrared (FTIR) Spectroscopy is a widely used analytical technique for identifying organic, polymeric, and some inorganic materials by measuring their infrared absorption spectra. The broader history of infrared spectroscopy, which serves as the foundation for its development, began with the 19th-century discovery of infrared radiation. However, it wasn't until the mid-1900s that advances in computation and interferometry made FTIR practical and widely used. The introduction of the Michelson interferometer and the use of Fourier transform methods to convert raw interferograms into spectral data revolutionised the field and made FTIR rapid, accurate, and suitable for daily research.

The theoretical foundation of FTIR is the interplay between matter and infrared radiation. Molecules absorb specific infrared light frequencies that match the energies of their vibrational transitions, such as the twisting, bending, or stretching of chemical bonds. Each material has

a unique set of vibrational modes that combine to form an infrared spectrum, which is a unique absorption pattern. Unlike classical dispersive IR spectroscopy, which scans over each wavelength independently, FTIR uses an interferometer to collect data simultaneously across all IR wavelengths. The resulting raw data, a complex signal that displays the light intensity as a function of the moving mirror's position within the interferometer, is called an interferogram.

An FTIR spectrometer directs an infrared radiation beam through a Michelson interferometer, where a beam splitter separates the beam into two paths: one path reflects off a moving mirror, and the other path reflects off a stationary mirror. The sample is traversed by the interference-patterned recombined beam. When specific infrared wavelengths are absorbed by the sample, the interferogram is altered. The final spectrum is produced by processing the modified signal using computer algorithms after it has been detected by a detector. The vibrational frequencies of the chemical bonds present in the sample are matched by the absorption peaks in this spectrum. FTIR can be used in transmission, reflectance, or attenuated total reflectance (ATR) modes, depending on the sample type and the information being sought.



**Figure 2.6.** A spectrometer for recording FT-IR spectrum.

## 2.7 Thermogravimetric and differential thermal analyses

Thermal analysis techniques known as thermogravimetric analysis (TGA) and differential thermal analysis (DTA) are used to examine, under controlled conditions, the physical and chemical changes of materials as a function of temperature or time. These methods have been refined and developed since the mid-1900s to provide valuable information about the phase transitions, composition, and thermal stability of a variety of materials, including metals, polymers, ceramics, and pharmaceuticals.

TGA is based on measuring the mass of a sample while it is heated, cooled, or maintained isothermally in a controlled atmosphere, usually air, nitrogen, or another inert gas. Thermal processes that cause the sample to lose mass or, less frequently, gain mass as the temperature rises include dehydration, decomposition, oxidation, and volatilisation. The result of continuously recording these changes is a thermogram, which is a plot of mass against temperature or time. The locations of mass changes help identify the composition of multi-component systems, thermal stability, and decomposition temperatures. For example, the mass loss steps in TGA can be used to estimate moisture content, filler percentages, or thermal breakdown pathways.



**Figure 2.7.** Set-up for TGA.



DTA, on the other hand, measures the temperature differential between a sample and an inert reference material using the same thermal cycle. When a thermal event occurs, like melting, crystallisation, or a chemical reaction, the sample either absorbs or releases heat, causing its temperature to differ from the reference. This temperature differential is displayed as a function of time or temperature using a DTA curve. The endothermic or exothermic peaks on the curve correspond to phase shifts or chemical processes, which are used to determine melting points, glass transitions, crystallisation behaviour, and reaction enthalpies.

A furnace equipped with a temperature controller and a high-precision balance is frequently included with both TGA and DTA equipment. In certain systems, TGA and DTA can be combined, often in conjunction with Differential Scanning Calorimetry, or DSC, to provide a more comprehensive thermal profile of the material. TGA gives quantitative data about weight changes, whereas DTA gives qualitative information about the thermal processes causing those changes.

## **2.8 Temperature-dependent photoluminescence spectroscopy**

Temperature-dependent photoluminescence (TDPL) spectroscopy is an enhanced version of conventional photoluminescence (PL) spectroscopy that investigates the temperature-dependent changes in a material's optical emission properties. It is especially helpful in semiconductor physics, nanomaterials research, and optoelectronic device characterisation because it provides insights into fundamental processes like carrier recombination dynamics, exciton behaviour, defect states, and band structure changes.



**Figure 2.8.** Spectrometer to acquire TD-PL spectrum.



The theoretical basis of TDPL is the temperature sensitivity of vibrational and electronic interactions within a material. When a light source, typically a laser, excites a semiconductor or insulator, electrons are transferred from the valence band to the conduction band. As they return to lower energy states, they release photons, which produces the photoluminescence signal. Numerous significant effects of temperature on this process include altering the occupation probability of defect or impurity states, triggering phonon-based non-radiative recombination pathways, broadening emission peaks as a result of increased lattice vibrations, and altering the band gap energy (which generally decreases with increasing temperature). As a result, the spectrum structure, intensity, and peak position of the PL emission vary with increasing temperature.

To perform TDPL spectroscopy, the sample is placed inside a cryostat, a device that can precisely adjust temperature, typically from cryogenic ( $\sim 4$  K) to room temperature and beyond. The sample is excited by a laser source, and the PL that is released is collected and transmitted to a detector and spectrometer, usually a CCD. By progressively altering the temperature and capturing spectra at each step, scientists build a dataset that illustrates how electronic transitions and recombination mechanisms change thermally.

# **CHAPTER 3**

## **EXPERIMENTAL PROCEDURE**

## CHAPTER 3: EXPERIMENTAL PROCEDURE

### 3.1 Synthesis of samples

Using a conventional high-temperature solid-state reaction method, dysprosium ion-doped CaYW phosphors were synthesised, where  $\text{Dy}^{3+}$  was taken in varying concentrations: 1 mol%, 3 mol%, 5 mol%, 7 mol%, 9 mol%, and 11 mol%. An electrical balance was used to weigh the highly pure precursors,  $\text{CaCO}_3$ ,  $\text{Y}_2\text{O}_3$ ,  $\text{WO}_3$ , and  $\text{Dy}_2\text{O}_3$ , in proper stoichiometric ratios precisely. After that, these reactants were properly mixed and ground in an agate mortar using a pestle for 1 h to obtain a homogeneous mixture. Then, the resultant chemical mixtures were put into alumina crucibles, and they were sintered in an electric furnace for 10 h at  $1100^\circ\text{C}$ . The samples were left to cool naturally to room temperature following the heating treatment. To improve homogeneity, the sintered products were then ground for about 10 to 15 min. Subsequently, further characterisations were carried out on the as-prepared phosphor samples.



**Figure 3.1.** Precursor chemicals were ground for 1 hour (on the left side), and they were stored in collection test-tubes (on the right side).

### 3.2 Instrumentation

Making use of a Bruker D-8 Advance diffractometer equipped with a nickel filter and  $\text{CuK}\alpha$  radiation ( $\lambda = 1.54 \text{ \AA}$ ), structural characterisation was carried out using x-ray diffraction (XRD). Data was gathered between  $10^\circ$  and  $90^\circ$  in a  $2\theta$  range. A JEOL 7610 F Plus scanning electron microscope (SEM) was used to investigate the morphological structures of the phosphor powders. A PerkinElmer Frontier spectrometer was employed to record Fourier transform-infrared (FT-IR) spectra. The optical band gap values were estimated using diffuse reflectance spectroscopy (DRS) data acquired using a JASCO V-770 spectrophotometer. A JASCO FP-8300 spectrofluorometer was used to acquire the photoluminescence (PL)

excitation and emission spectra, with a xenon lamp serving as the excitation source. Using a PerkinElmer TGA system, thermogravimetric analysis (TGA) was used to analyse thermal behaviour. Temperature dependent-photoluminescence (TD-PL) spectra were recorded using an Ocean Optics spectrometer equipped with an integrated heating unit.



**Figure 3.2.** Furnace.

# **CHAPTER 4**

## **RESULTS AND DISCUSSION**

## CHAPTER 4: RESULTS AND DISCUSSION

### 4.1 X-ray diffraction (XRD) analysis

The samples' crystal structure was determined by analysing the x-ray diffraction (XRD) patterns. Figure 4.1 represents the patterns for undoped CaYW, CaYW:9mol%Dy<sup>3+</sup>, and standard JCPDS 38-0218. For the undoped CaYW sample, the diffraction peaks are sharp and intense, indicating good crystallinity. For the Dy-doped CaYW sample, peak positions closely match those of both the undoped sample and the JCPDS reference. The intensities of some peaks are slightly altered, which can be attributed to preferred orientation changes due to Dy<sup>3+</sup> doping and slight lattice distortion from Dy<sup>3+</sup> (ionic radius ~1.03 Å) replacing Y<sup>3+</sup> (ionic radius ~1.019 Å). Thus, the close resemblance of the patterns of undoped and doped samples with the JCPDS pattern concludes that their crystal structure is tetragonal.

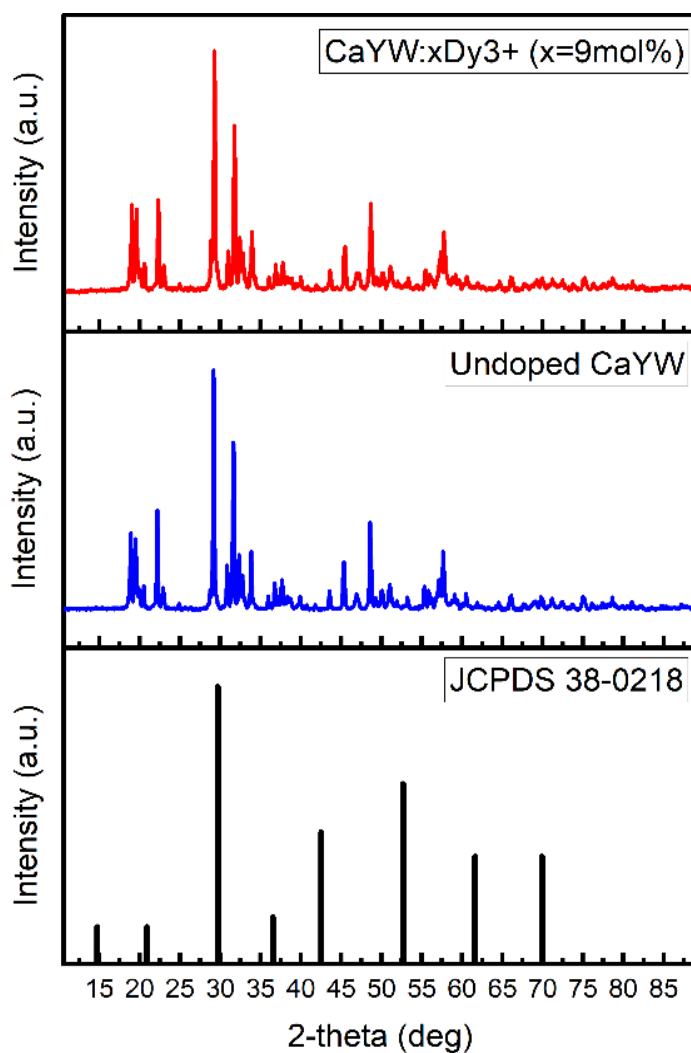


**Figure 4.1.** X-ray diffraction (XRD) patterns for undoped CaYW and CaYW:9mol%Dy<sup>3+</sup>, along with the JCPDS pattern.

Using the Debye-Scherrer formula, the crystallite size was calculated from the most noticeable diffraction peaks [13,14].

$$D = \frac{k\lambda}{\beta \cos \theta} \quad (1)$$

Here, x-ray wavelength is denoted by  $\lambda$ , full width at half maximum (FWHM) of the diffraction peak is represented by  $\beta$ , Bragg angle is denoted by  $\theta$ , crystallite size is symbolised by  $D$ , and shape factor is denoted by  $K$  (0.94). Thus, the average crystallite size was estimated to be 313.2 nm.

#### 4.2 Scanning electron microscopic (SEM) analysis

This analysis was conducted to study the morphological aspects of the as-prepared samples. Figure 4.2 represents the micrographs of: (a) undoped CaYW and (b) CaYW:9mol%Dy<sup>3+</sup>.

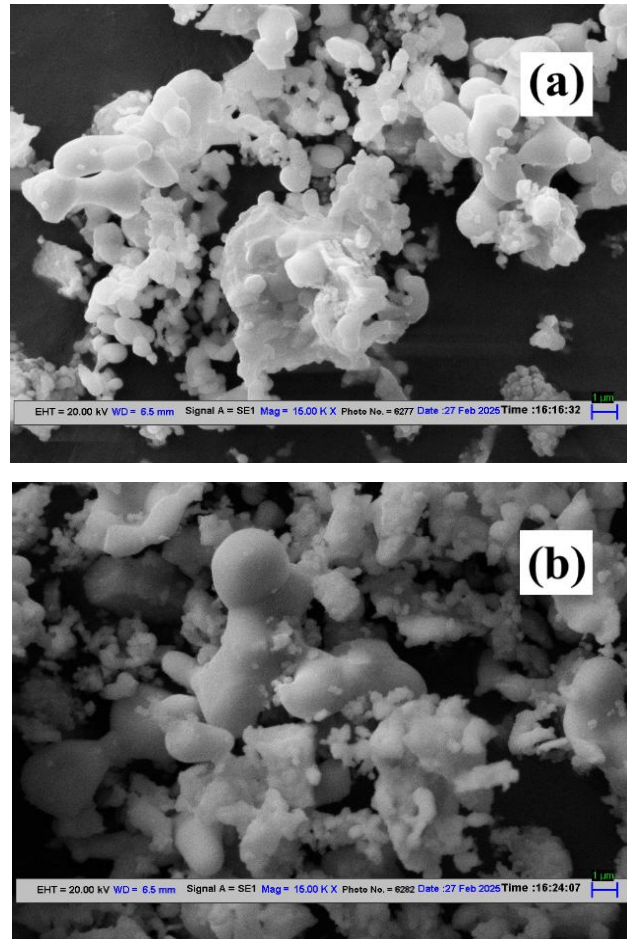


**Figure 4.2.** (a) SEM image for undoped CaYW, (b) SEM image for CaYW:9mol%Dy<sup>3+</sup>.

The images display that for the undoped CaYW, the particles are more finely dispersed, with smaller grain sizes compared to the doped counterpart, and grain boundaries are more

distinguishable, suggesting better separation and less fusion among particles. The size of the particles was estimated within the range of 1–5  $\mu\text{m}$ . Also, for CaYW:9mol%Dy<sup>3+</sup> phosphor, the microstructure exhibits larger, well-fused, and agglomerated particles. There is noticeable spherical grain morphology, with some smooth and bulky aggregates. Agglomeration is stronger, possibly due to the presence of dopant ions (Dy<sup>3+</sup>), which can influence grain growth and particle interaction during synthesis. The size of the particles was estimated within the range of 1–7  $\mu\text{m}$ .

### 4.3 Diffuse reflectance spectroscopic (DRS) analysis

Figure 4.3(a) illustrates the diffuse reflectance spectra for the undoped and Dy-doped CaYW samples, which were examined within the 200–1500 nm range. The Dy-doped CaYW phosphors' spectra show a reflectance within the range of 300–400 nm, which corresponds to band gap absorption—electrons get excited, and they move from the valence band to the conduction band. In addition to this, the spectra exhibit that the reflectance dips correspond to transitions from <sup>6</sup>H<sub>15/2</sub> (ground level) to <sup>4</sup>M<sub>15/2</sub>, <sup>6</sup>F<sub>3/2</sub>, <sup>6</sup>F<sub>5/2</sub>, <sup>6</sup>F<sub>7/2</sub>, and <sup>6</sup>H<sub>7/2</sub> (excited levels) [15–17]. The dips in reflectance in the visible and near-infrared (IR) regions correspond to d-d transitions, which become more prominent with the increase in dopant ion concentration. Also, the noticeable dips in the infrared (IR) region likely correspond to f-f transitions within the dopant ions' 4f orbitals, which become more prominent with an increase in doping.

The Kubelka-Munk function, which describes the optical absorption close to the band edge, was used to compute the optical band gap values [18,19]:

$$F(R)hv = C(hv - E_g)^{n/2} \quad (2)$$

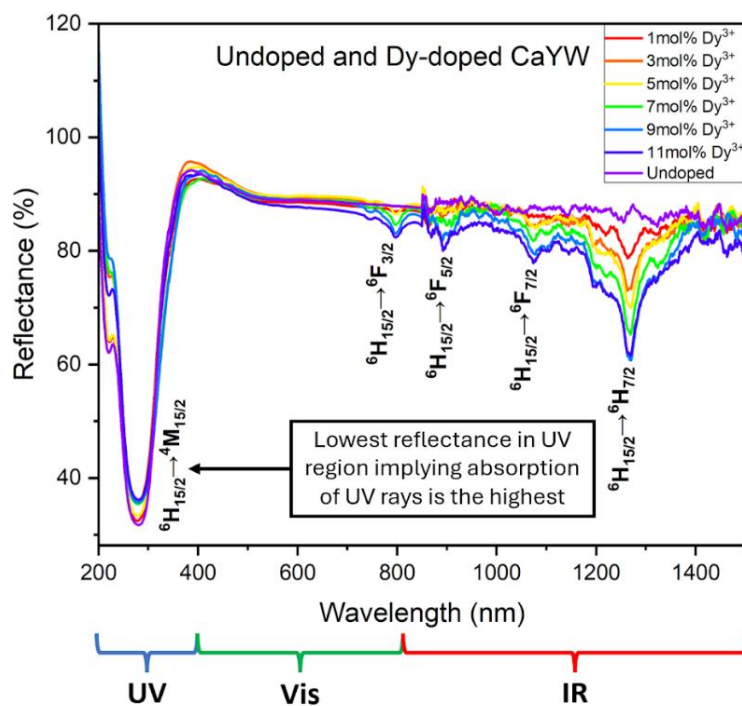
where  $hv$  is the photon energy,  $E_g$  denotes the energy band gap, and  $C$  is a constant. For direct transition,  $n=1$ , and for indirect transition,  $n=4$ .

The function  $(R)$  can be expressed as [20,21]:

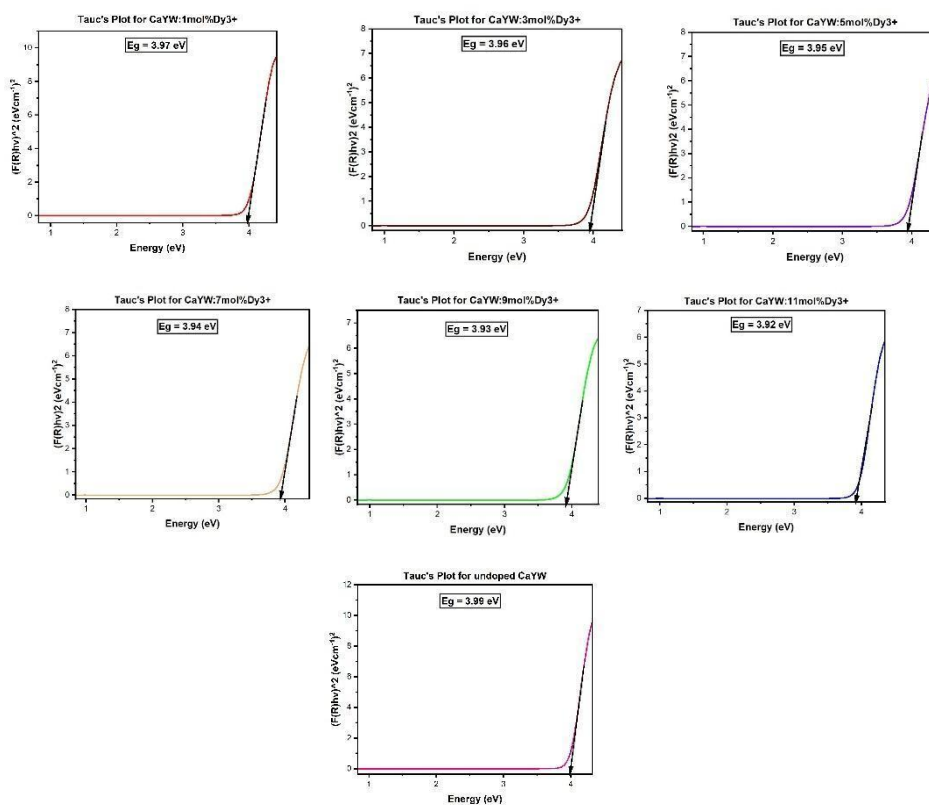
$$F(R) = \frac{(1-R)^2}{2R} = \frac{\alpha}{S} \quad (3)$$

where  $R$  represents the reflectance,  $\alpha$  represents the absorbance, and  $S$  is the scattering coefficient. Figure 4.3(b) illustrates the optical band gap values for the undoped and doped CaYW samples. These values were estimated from the extrapolation of the linear portion of data between  $[F(R)hv]^2$  and  $hv$ .





(a)



(b)

**Figure 4.3.** (a) Diffuse reflectance spectra for undoped and Dy-doped CaYW samples, (b) Tauc's plots for direct bandgap of undoped CaYW and doped CaYW phosphors.

Table I consists of the band gap energy data along with corresponding dopant ion concentrations.

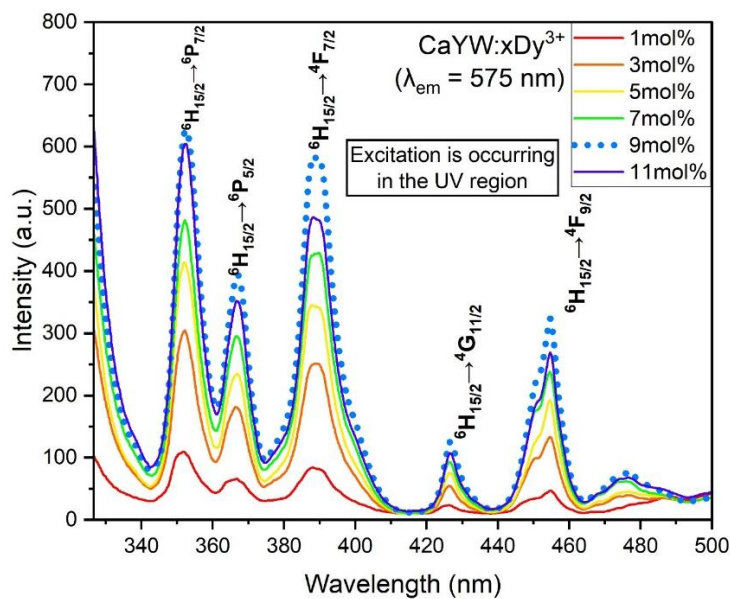
**Table I.** Bandgap energy data for undoped CaYW and CaYW:xDy<sup>3+</sup> phosphors.

x (in mol%)	E <sub>g</sub> (in eV)
0	3.99
1	3.97
3	3.96
5	3.95
7	3.94
9	3.93
11	3.92

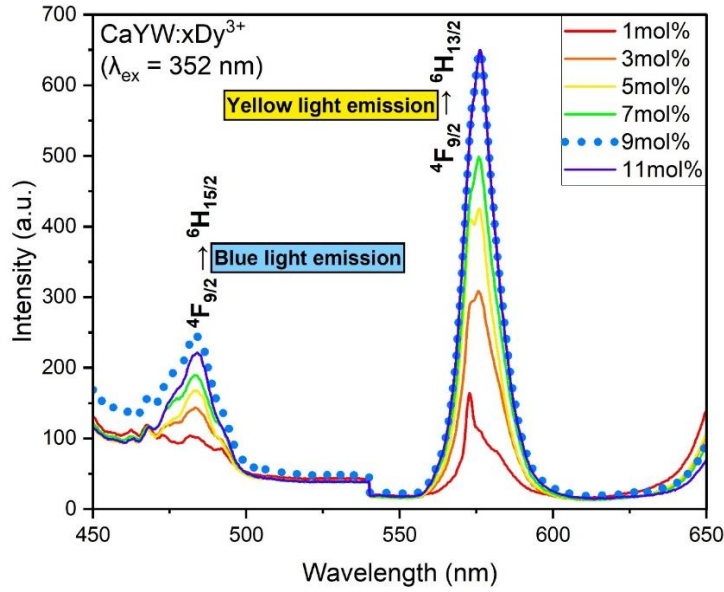
Thus, from Figure 3(b) and Table I, it is evident that the optical band gap value ( $E_g$ ) decreases from 3.99 eV to 3.92 eV as the concentration of Dy<sup>3+</sup> ions increases from 0 to 11 mol%. This can be attributed to the 4f energy levels of Dy<sup>3+</sup> ions.

#### 4.4 Photoluminescence (PL) spectral analysis

The graph of photoluminescence (PL) excitation spectra for the CaYW:xDy<sup>3+</sup> (1, 3, 5, 7, 9, and 11 mol%) phosphors recorded at an emission wavelength of 575 nm ( $\lambda_{em}$ ) within the 325–500 nm range has been displayed in Figure 4.4(a).



(a)



(b)

**Figure 4.4** (a) Photoluminescence (PL) excitation spectra for all the Dy<sup>3+</sup>-doped CaYW phosphors, (b) emission spectra for the same samples.

In the given spectra, there are several prominent peaks, indicating 4f-4f electronic transitions of the Dy<sup>3+</sup> ion from the ground electronic state to higher-energy excited states. Here, all the peaks are at: 352 nm ( $^6H_{15/2} \rightarrow ^6P_{7/2}$ ), 367 nm ( $^6H_{15/2} \rightarrow ^6P_{5/2}$ ), 391 nm ( $^6H_{15/2} \rightarrow ^4F_{7/2}$ ), 427 nm ( $^6H_{15/2} \rightarrow ^4G_{11/2}$ ), and 455 nm ( $^6H_{15/2} \rightarrow ^4F_{9/2}$ ) [22–25]. And the peak at 352 nm corresponds to highest intensity value.

The graph of photoluminescence (PL) emission spectra for the same phosphors, recorded at an excitation wavelength of 352 nm ( $\lambda_{ex}$ ), within the 450–650 nm range, is displayed in Figure 4.4(b). In the given spectra, there are two prominent peaks: 486 nm (blue light emission), corresponding to  $^4F_{9/2} \rightarrow ^6H_{15/2}$  transition, and 575 nm (yellow light emission), corresponding to  $^4F_{9/2} \rightarrow ^6H_{13/2}$  transition. These transitions are related to electric and magnetic dipoles. At 575 nm, the peak with the strongest emission intensity was observed.

From Figure 4.4(b), it may be noted that the photoluminescence (PL) intensity of the phosphors gradually increases up to 9 mol% of Dy<sup>3+</sup> ions. However, the emission intensity decreases as the dopant concentration is increased further. This phenomenon is attributed to concentration quenching, i.e., as the concentration of Dy<sup>3+</sup> ions within the host lattice increases, the distances between the ions decrease. After a certain concentration is reached, the proximity among the ions promotes nonradiative energy transfer between excited and unexcited ions,

which results in the lowering of the photoluminescence (PL) efficiency. Therefore, it can be concluded that the optimum concentration for  $\text{CaYW}:\text{x}\text{Dy}^{3+}$  where  $\text{x} = 9 \text{ mol}\%$ .

#### 4.5 Commission Internationale de l'Éclairage (CIE) coordinates and correlated colour temperature (CCT) analysis

The Commission Internationale de l'Éclairage (CIE) coordinates offer important information about the colour properties of the light that a phosphor emits. The CIE Chromaticity coordinates used in this study were obtained from the CIE 1931 chromaticity diagram. These coordinates are a useful way to analyse a phosphor's luminous efficiency. The coordinates for the as-prepared phosphors, which were obtained from the photoluminescence (PL) emission spectra under excitation at 352 nm, were evaluated, and they have been tabulated in Table II. Also, in Figure 4.5, a chromaticity diagram has been used to illustrate the location of the optimum phosphor sample,  $\text{CaYW}:\text{9mol}\%\text{Dy}^{3+}$ , whose CIE coordinates have been labelled.

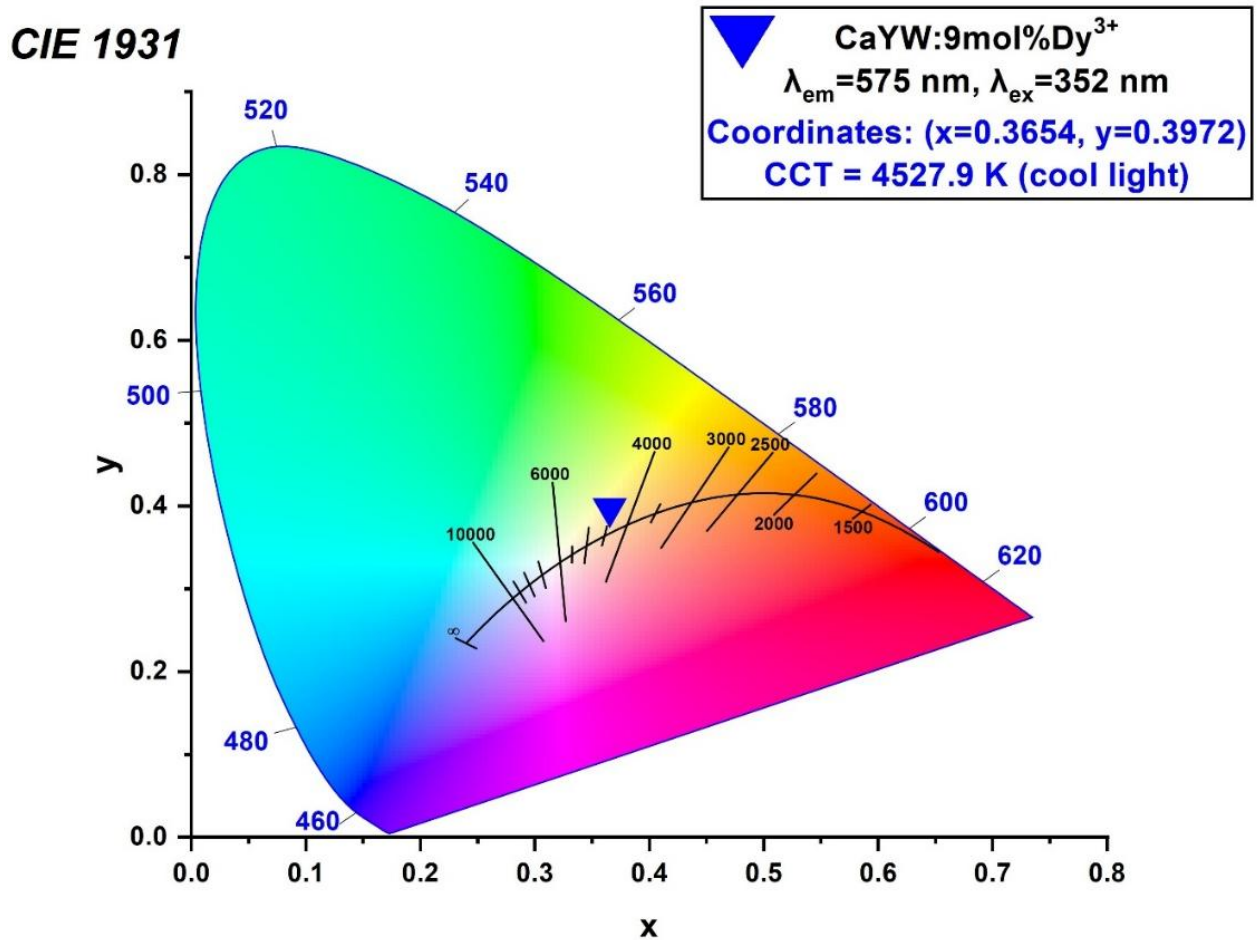


**Figure 4.5.** Chromaticity diagram for  $\text{CaYW}:\text{9mol}\%\text{Dy}^{3+}$  phosphor sample.

**Table II.** CIE coordinates for CaYW:xDy<sup>3+</sup> phosphors.

x (in mol%)	(CIE x, CIE y)
1	(0.2895, 0.3198)
3	(0.3287, 0.3609)
5	(0.3459, 0.3789)
7	(0.3520, 0.3829)
9	(0.3654, 0.3972)
11	(0.3479, 0.3766)

It is to be noted that the coordinates for the optimum sample are falling in the yellowish-white region. Thus, this phosphor has the potential to be used in white light-emitting diodes.

Another parameter is studied, other than these coordinates, which is known as correlated colour temperature (CCT). It determines whether a luminous source seems warm or cool: for which the reference luminous source is heated to some temperature (in Kelvin), and it releases light that is compared with the given luminous source. While luminous sources with CCT values below 3500 K are considered warm, the ones with CCT values above 4000 K are regarded as cool. The CCT value for the optimum sample was evaluated using McCamy's relation [26,27].

$$CCT = -449n^3 + 3525n^2 - 6823.2n + 5520.3 \quad (4)$$

where  $n = \frac{(x-x_e)}{(y-y_e)}$  and  $x_e = 0.332$  &  $y_e = 0.186$ . Thus, the CCT value for the optimum phosphor sample was calculated using equation (4), and it was found to be 4527.9 K, which indicates a cool luminous source.

#### 4.6 Fourier transform-infrared spectroscopic (FT-IR) analysis

This analysis looked at the type of bond interactions and functional groups that could be present in the undoped host matrix and optimum phosphor sample. The Fourier transform-infrared (FT-IR) spectra for both the samples were obtained in the 450–4000 cm<sup>-1</sup> range. In Figure 4.6, several characteristic vibrational bands can be seen at 472, 722, 946, 1418, and 3644 cm<sup>-1</sup>. The metal-oxygen stretching and bending vibrations involving Y-O and W-O bonds can be ascribed to the bands at 472 cm<sup>-1</sup> and 722 cm<sup>-1</sup> [28–30]. The absorption band at 946 cm<sup>-1</sup> corresponds to the stretching vibrations of terminal W=O bonds. The dip at 1418 cm<sup>-1</sup> is characteristic of

asymmetric bending vibrations of the  $\text{CO}_3^{2-}$  group [31]. The stretching vibration mode of O-H is represented by the band at  $3466\text{ cm}^{-1}$  [32]. The presence of the OH group suggests the increase in non-radiative loss that, in turn, can lower the quantum efficiency of the material. Here, the band displaying OH group is quite weak, which means that its concentration is very little in the doped sample. From these results, it is evident that several different functional groups are same in both the samples, and only the intensity of peaks changes while the peak profile stays unchanged. Thus, the spectra indicate that  $\text{Dy}^{3+}$  ions have been successfully incorporated into the host matrix.

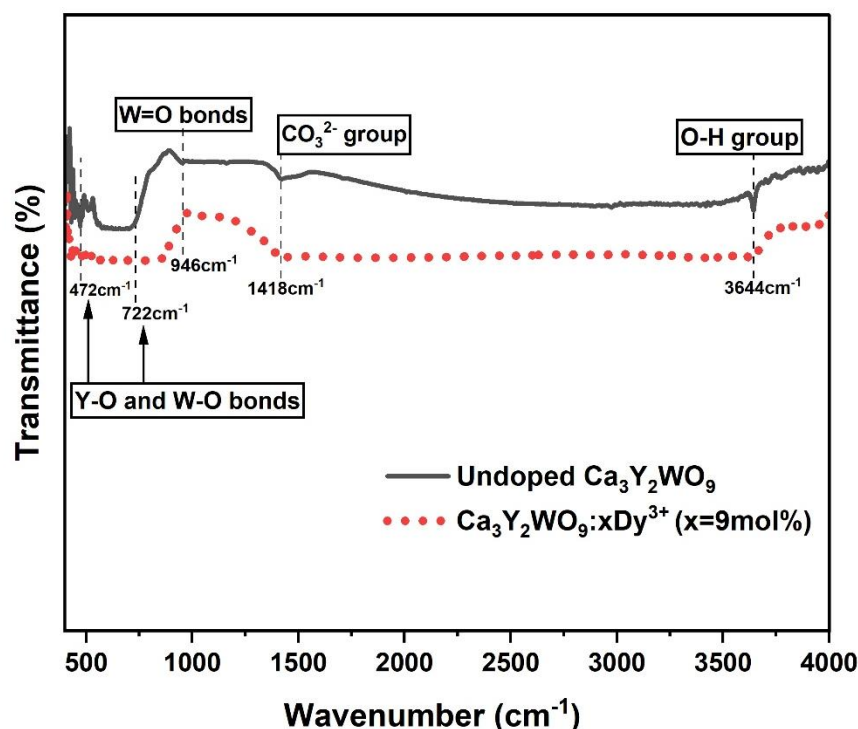


**Figure 4.6.** Fourier transform-infrared (FT-IR) spectra for undoped and 9 mol%  $\text{Dy}^{3+}$ -doped CaYW samples.

#### 4.7 Thermogravimetric analysis (TGA) and differential thermal analysis (DTA)

Thermogravimetric analysis (TGA) helps us in understanding the thermal properties of the as-prepared undoped host matrix. Analysing the TGA curve given in Figure 4.7 of the undoped CaYW within the temperature range of 28– $1000^\circ\text{C}$ , weight loss can be observed in two prominent regions. The first stage of weight loss of 4.21% is displayed over a temperature range of 200– $600^\circ\text{C}$ . It likely arises due to removal of absorbed moisture or minor carbonate decomposition. Another stage of weight loss of about 12.69% is evident in the range 600– $800^\circ\text{C}$  that corresponds to major decomposition event including volatile oxide burnout. No

significant mass loss is visible after this region signifying the beginning of pure phase formation of CaYW and the end point of calcination process.

The differential thermal analysis (DTA) curve identifies the weight loss process during the formation of pure CaYW phase. The endothermic peak observed at 778°C is assigned to rapid mass loss region in the given graph. It attributes to phase transformation of the host matrix leading to the formation of a thermally stable CaYW host matrix [33–39].

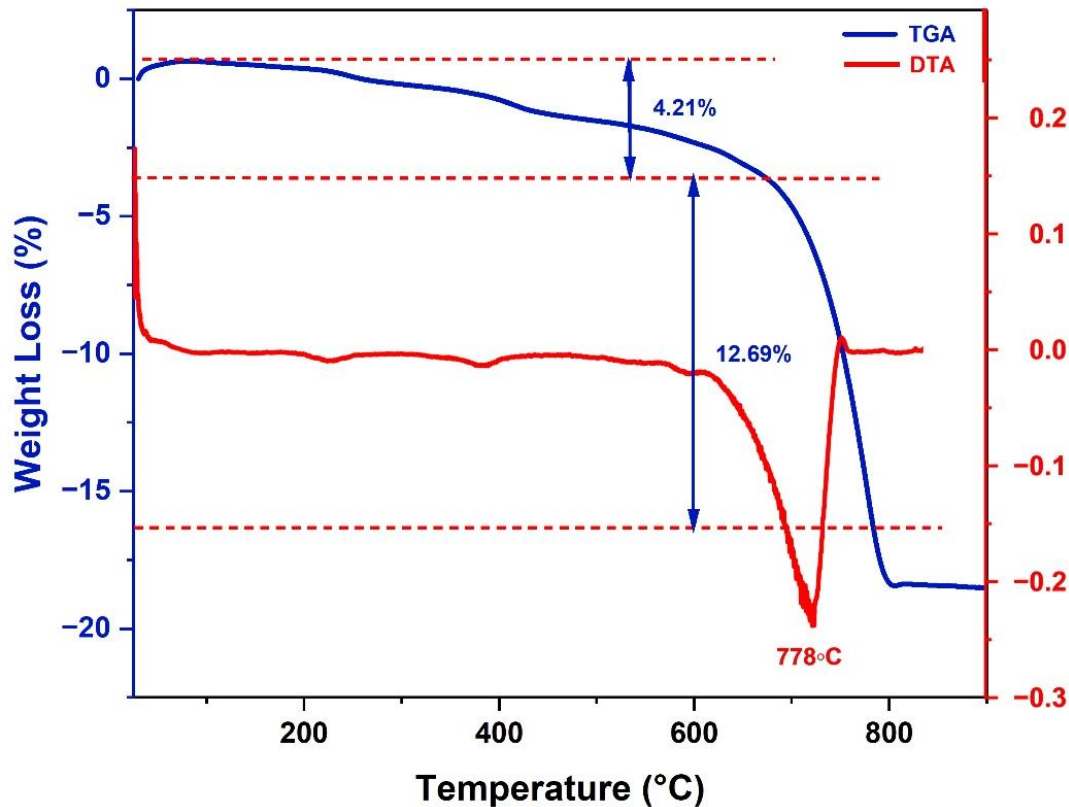


**Figure 4.7.** Thermogravimetric and differential curves for CaYW host matrix.

#### 4.8 Temperature dependent-photoluminescence (TD-PL) spectral analysis

The thermal quenching properties of CaYW:9mol%Dy<sup>3+</sup> phosphor were analysed by observing the temperature dependent-photoluminescence (TD-PL) spectra measured at  $\lambda_{ex} = 352$  nm within the temperature range of 28–175°C. With the rise in temperature, the intensities of the photoluminescence (PL) bands were observed to be decreasing while the peak positions remained unchanged as illustrated in Figure 4.8. The phosphor's luminescence exhibits a drop due to non-radiative transition. The normalised intensity of the  $^4F_{9/2} \rightarrow ^6H_{11/2}$  transition concerning temperature, where the maximum emission intensity at 28°C is considered as 100%. From the plot, we can see a drop in emission intensity of about 9.72% making the emission



intensity reduce from 100% at 28°C to almost 91% at 175°C, indicating high thermal stability of the as-prepared phosphor sample.

The thermal quenching behaviour of the sample was further investigated by calculating the activation energy ( $\Delta E$ ) using the Arrhenius equation:

$$I_T = \frac{I_0}{1 + C \exp\left(-\frac{\Delta E}{K_B T}\right)} \quad (5)$$

where  $I_T$  and  $I_0$  are the PL intensities at initial temperature 28°C and temperature  $T$  (Kelvin), respectively,  $K_B$  is the Boltzmann constant, and  $C$  denotes the constant term. From the slope of the plot of  $\ln\left[\left(\frac{I_0}{I_T}\right) - 1\right]$  versus  $1/K_B T$  as shown in Figure 4.9, activation energy ( $\Delta E$ ) is calculated. The measured activation energy came out to be 0.260 eV which is higher than other values in literature [40–42]. Greater activation energy suggests higher thermal stability which vies for ideal use of the optimum phosphor in white light-emitting diodes [43–56].

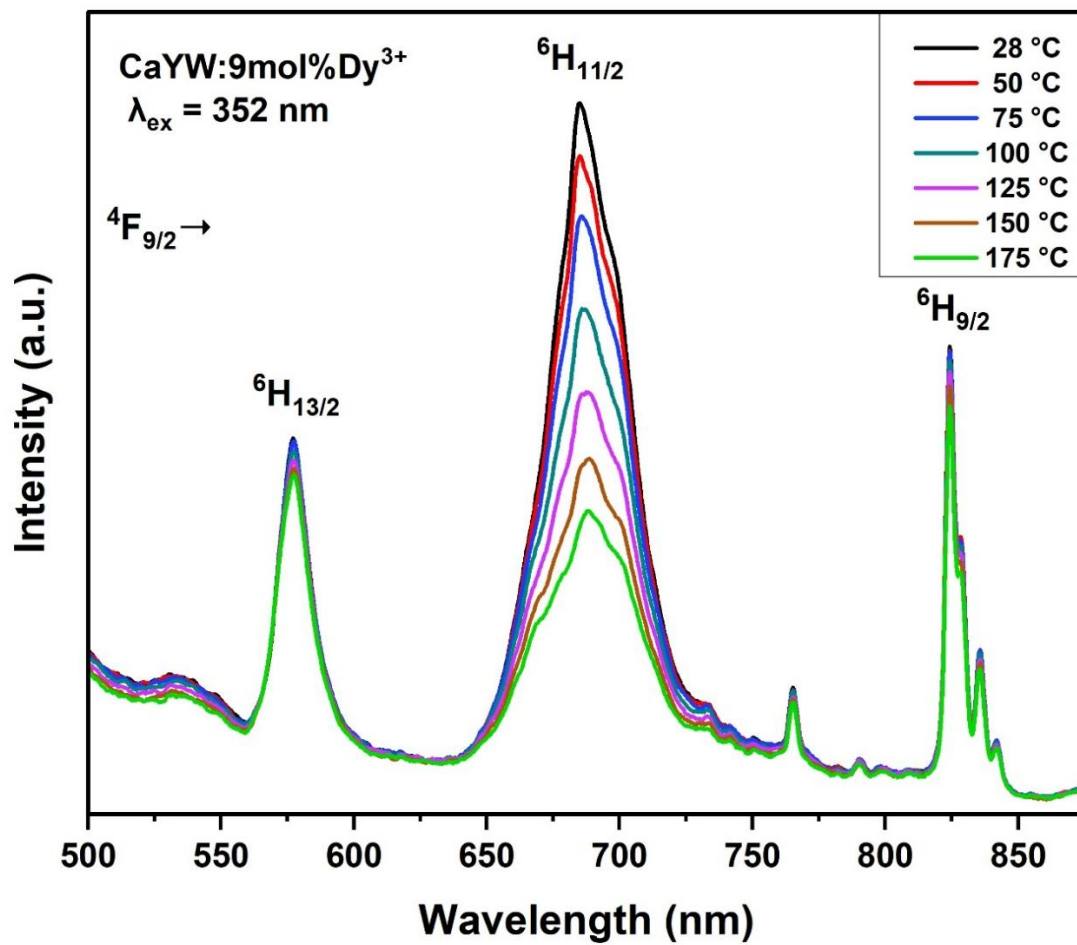


**Figure 4.8.** Temperature dependent-photoluminescence (TD-PL) spectra for CaYW:9mol%Dy<sup>3+</sup> phosphor at  $\lambda_{ex} = 352$  nm.



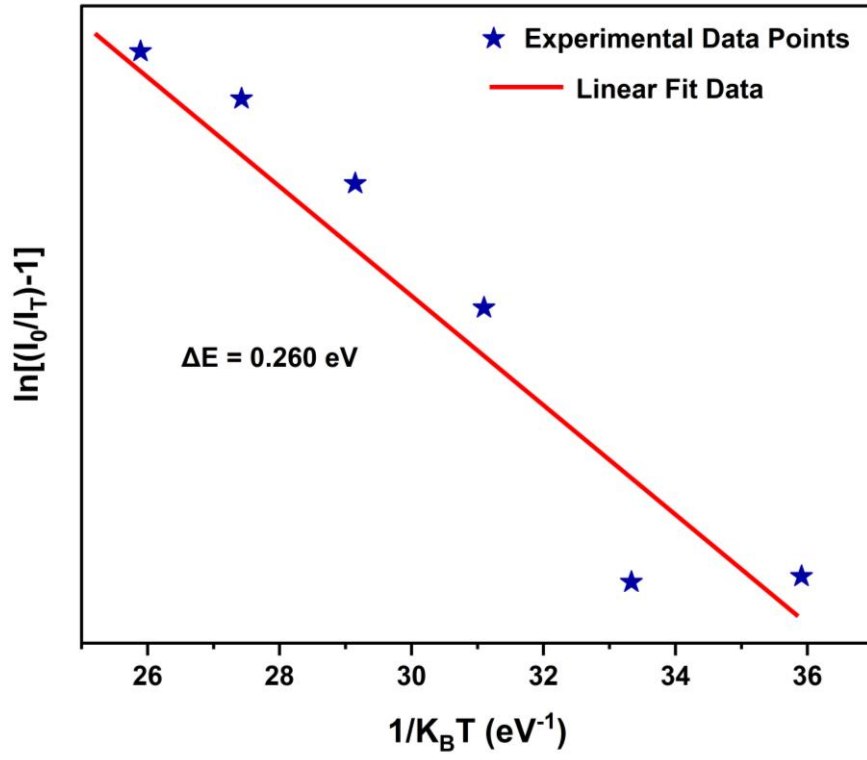


**Figure 4.9.** Linear plot of  $\ln[(\frac{I_0}{I_T}) - 1]$  vs  $1/K_B T$  to calculate the activation energy.

# CHAPTER 5

# CONCLUSION

## CHAPTER 5: CONCLUSION

A series of  $\text{Ca}_3\text{Y}_2\text{WO}_9:\text{x}\text{Dy}^{3+}$  doped phosphors ( $\text{x}=1, 3, 5, 7, 9$ , and  $11$  mol%) was synthesised utilising the solid-state reaction method at  $1100^\circ\text{C}$ . The crystal structure formation, luminescent properties, and other properties of the as-prepared phosphors had been studied using various characterisation techniques such as XRD, SEM, DRS, PL, and FT-IR. The crystalline nature, i.e., the tetragonal crystal structure of the as-prepared phosphors, had been confirmed through XRD analysis. After analysing the images obtained from SEM, the optimum synthesised sample was observed to be made up of very tiny and agglomerated particles ranging from  $1$  to  $7\ \mu\text{m}$ . The functional groups had been identified with the help of FT-IR spectra. The DRS results showed that when the concentration of  $\text{Dy}^{3+}$  ions increased, there was a little change in the bandgap, which indicated that doping did not influence the structure of the material. The phosphors' PL excitation spectra showed excitation peaks in the ultraviolet region of the electromagnetic spectrum, at an emission wavelength of  $575\ \text{nm}$ . The PL emission spectra showed two prominent emission peaks at  $486\ \text{nm}$  (blue light emission due to  $^4\text{F}_{9/2}\rightarrow^6\text{H}_{15/2}$  transition) and  $575\ \text{nm}$  (yellow light emission due to  $^4\text{F}_{9/2}\rightarrow^6\text{H}_{13/2}$  transition). Concentration quenching occurred after  $9$  mol% of  $\text{Dy}^{3+}$  ions, and the emission intensity decreased after it. The estimated CIE and CCT values indicated that the synthesised phosphors emitted yellowish-white light, which suggested that they can be used where white light is needed. TGA and DTA graph showed the pure phase formation of a thermally stable host matrix. From TD-PL results, the activation energy was measured to be  $0.260\ \text{eV}$ , which is higher than other values in previous studies, suggesting higher thermal stability. Finally, all the observed results point towards the possibility that the as-prepared phosphor samples have the potential to be used in w-LEDs.

## REFERENCES

- [1] Gaft, M., Reisfeld, R., & Panczer, G. (2023). Fluorescence and Phosphorescence Spectroscopies and Their Applications in Gem Characterization. *Minerals*, 13(5), 626. <https://doi.org/10.3390/min13050626>
- [2] Ye, S., Xiao, F., Pan, Y. X., Ma, Y. Y., & Zhang, Q. Y. (2014). Development of phosphors with high thermal stability and efficiency for phosphor-converted LEDs. *Journal of Solid State Lighting*, 1(1), 1-20. <https://doi.org/10.1186/s40539-014-0011-8>
- [3] Aitas, M., & Suresh, S. (2016). Persistent luminescence: An insight. *Renewable and Sustainable Energy Reviews*, 65, 135-153. <https://doi.org/10.1016/j.rser.2016.06.081>
- [4] Zhao, Y., & Xia, Z. (2021). Recent progress of effect of crystal structure on luminescence properties of  $\text{Ce}^{3+}$ – $\text{Eu}^{2+}$  co-doped phosphors. *RSC Advances*, 11(49), 30989–31008. <https://doi.org/10.1039/D1RA04700K>
- [5] Balakrishna, A., & Suresh, S. (2023). The Role of Anions in Rare-earth Activated Inorganic Host Materials for its Luminescence Characteristics. *Journal of Fluorescence*, 33, 1–17. <https://doi.org/10.1007/s10895-023-03561-0>
- [6] Van Uitert, L. G. (1967). Characterization of luminescent materials. *Journal of The Electrochemical Society*, 114(10), 1048. DOI: 10.1149/1.2424184
- [7] Zhang, S., Li, Y., Lv, Y., Fan, L., Hu, Y., & He, M. (2017). A full-color emitting phosphor  $\text{Ca}_9\text{Ce}(\text{PO}_4)_7\text{:Mn}^{2+}, \text{Tb}^{3+}$ : Efficient energy transfer, stable thermal stability and high quantum efficiency. *Chemical Engineering Journal*, 322, 314–327. DOI: 10.1016/j.cej.2017.04.032
- [8] Linderälv, C., Åberg, D., & Erhart, P. (2020). Luminescence quenching via deep defect states: A recombination pathway via oxygen vacancies in Ce-doped YAG. DOI: 10.1021/acs.chemmater.0c02449
- [9] Liu, H., Zhao, F., Cai, H., Song, Z., & Liu, Q. (2022). Consequence of optimal bonding on cation ordering and enhanced near-infrared luminescence in  $\text{Cr}^{3+}$ -doped pyroxene oxides. *Journal of Materials Chemistry C*, 10(24), 9232–9240. <https://doi.org/10.1039/D2TC01792J>
- [10] Wang, W., Yang, P., Gai, S., Niu, N., He, F., & Lin, J. (2010). Fabrication and luminescent properties of  $\text{CaWO}_4\text{:Ln}^{3+}$  ( $\text{Ln} = \text{Eu}, \text{Sm}, \text{Dy}$ ) nanocrystals. *Journal of Nanoparticle Research*, 12(8), 2295–2305. <https://doi.org/10.1007/s11051-010-9850-4>
- [11] Tang, S., Gao, H., Wang, S., Yu, C., Chen, X., Liu, H., Gao, Q., Yu, X., Zhao, X., & Sun, G. (2022). Temperature Dependence of the Phase Transformation and Photoluminescence Properties of Metastable  $\text{ZnWO}_4$  Nano-Phosphors with High UV Absorption and VIS Reflectance. *Russian Journal of Physical Chemistry A*, 96(3), 515–526. <https://doi.org/10.1134/S0036024422030220>

- [12] (2006). Instrumentation for Fluorescence Spectroscopy. In: Lakowicz, J.R. (eds) Principles of Fluorescence Spectroscopy. Springer, Boston, MA. [https://doi.org/10.1007/978-0-387-46312-4\\_2](https://doi.org/10.1007/978-0-387-46312-4_2)
- [13] P. Kumar, S. Singh, I. Gupta, K. Nehra, V. Kumar, D. Singh, Structural and luminescent behaviour of Dy(III) activated Gd<sub>3</sub>Al<sub>5</sub>O<sub>12</sub> nanophosphors for white-LEDs applications, Mater. Chem. Phys. 295 (2023) 127035, <https://doi.org/10.1016/j.matchemphys.2022.127035>.
- [14] R. Kokate, P. Rohilla, S. Kaur, A.S. Rao, V. Singh, Visible emission characteristics in Tb<sup>3+</sup>-doped KNa<sub>3</sub>Al<sub>4</sub>Si<sub>4</sub>O<sub>16</sub> phosphor, Optik 243 (2021) 167391, <https://doi.org/10.1016/j.ijleo.2021.167391>.
- [15] W.T. Carnall, P.R. Fields, K. Rajnak, Electronic energy levels of the trivalent lanthanide aquo ions. III. Tb<sup>3+</sup>, J. Chem. Phys. 49 (1968) 4447–4449, <https://doi.org/10.1063/1.1669895>.
- [16] W.T. Carnall, P.R. Fields, K. Rajnak, Electronic energy levels of the trivalent lanthanide aquo ions. IV. Eu<sup>3+</sup>, J. Chem. Phys. 49 (1968) 4450–4455, <https://doi.org/10.1063/1.1669896>.
- [17] C.R. Kesavulu, H.J. Kim, S.W. Lee, J. Kaewkhao, N. Chanthima, Y. Tariwong, Physical, vibrational, optical and luminescence investigations of Dy<sup>3+</sup>-doped yttrium calcium silicoborate glasses for cool white LED applications, J. Alloys Compd. 726 (2017) 1062–1071, <https://doi.org/10.1016/j.jallcom.2017.08.091>.
- [18] R.R. Cui, X. Guo, X.Y. Gong, C.Y. Deng, Photoluminescence properties and energy transfer of novel orange–red emitting phosphors: Ba<sub>3</sub>Bi<sub>2</sub>(PO<sub>4</sub>)<sub>4</sub>: Sm<sup>3+</sup>, Eu<sup>3+</sup> for white light-emitting diodes, Rare Met. 40 (2021) 2882–2891, <https://doi.org/10.1007/s12598-020-01663-3>.
- [19] E.A. Rathnakumari, S.M.M. Kennedy, Photoluminescence properties of certain trivalent RE ions (Dy/Sm/Eu) activated NaSrBi<sub>2</sub>(PO<sub>4</sub>)<sub>3</sub> phosphors and cool to warm white color tuning in Dy<sup>3+</sup>- Sm<sup>3+</sup> and Dy<sup>3+</sup>- Eu<sup>3+</sup> codoped NaSrBi<sub>2</sub>(PO<sub>4</sub>)<sub>3</sub> phosphors for indoor lighting applications, J. Lumin. 235 (2021) 118018, <https://doi.org/10.1016/j.jlumin.2021.118018>.
- [20] K.C. Sushma, R.B. Basavaraj, D.P. Aarti, M.B.M. Reddy, G. Nagaraju, M. S. Rudresha, H.M.S. Kumar, K.N. Venkatachalaiah, Efficient red-emitting SrZrO<sub>3</sub>:Eu<sup>3+</sup> phosphor superstructures for display device applications, J. Mol. Struct. 1283 (2023) 135192, <https://doi.org/10.1016/j.molstruc.2023.135192>.
- [21] K.S. Rao, B.V.N. Kumar, Y.N. Rajeev, K. Venkatarao, S. Cole, Structural, morphological and photoluminescence properties of Eu<sup>3+</sup> doped Cd<sub>2</sub>Sr(PO<sub>4</sub>)<sub>2</sub> nanopowder, J. Mol. Struct. 1284 (2023) 135406, <https://doi.org/10.1016/j.molstruc.2023.135406>.

- [22] D. Kavyashree, D.R. Lavanya, H. Nagabhushana, D. V Sunitha, Solution combustion synthesis of Dy<sup>3+</sup> doped La<sub>2</sub>O<sub>3</sub> nanoparticles: an investigation of their structural, optical and photoluminescence characteristics, *Inorg. Chem. Commun.* 160 (2024) 111910, <https://doi.org/10.1016/j.inoche.2023.111910>.
- [23] A. Gaikwad, Y.R. Parauha, K. V Dabre, S.J. Dhoble, Improvement in spectroscopic properties of Dy<sup>3+</sup> doped Ba<sub>2</sub>Mg(PO<sub>4</sub>)<sub>2</sub> phosphors through substitution strategy, *Mater. Today Commun.* 37 (2023) 107247, <https://doi.org/10.1016/j.mtcomm.2023.107247>.
- [24] W. Tang, Q. Guo, K. Su, H. Liu, Y. Zhang, L. Mei, L. Liao, Structure and photoluminescence properties of Dy<sup>3+</sup> doped phosphor with whitlockite structure, *Materials* 15 (2022) 4–13, <https://doi.org/10.3390/ma15062177>.
- [25] N. Can, M.B. Coban, G. Souadi, Ü.H. Kaynar, M. Ayvacikli, J. Garcia Guinea, E. Ekdal Karali, Synthesis, characterization and enhanced photoluminescence and temperature dependence of ZrO<sub>2</sub>:Dy<sup>3+</sup> phosphors upon incorporation of K<sup>+</sup> ions, *Ceram. Int.* 49 (2023) 36752–36762, <https://doi.org/10.1016/j.ceramint.2023.09.003>.
- [26] C.S. McCamy, Correlated color temperature as an explicit function of chromaticity coordinates, *Color Res. Appl.* 17 (1992) 142–144, <https://doi.org/10.1002/col.5080170211>.
- [27] C.B.A. Devi, K. Swapna, S. Mahamuda, M. Venkateswarlu, M.V.V.K.S. Prasad, K. Siva Rama Krishna Reddy, N. Deopa, A.S. Rao, Spectroscopic studies and lasing potentialities of Sm<sup>3+</sup> ions doped single alkali and mixed alkali fluoro tungstentellurite glasses, *Opt. Laser Technol.* 111 (2019) 176–183, <https://doi.org/10.1016/j.optlastec.2018.09.051>.
- [28] Wang, Y., Zhang, L., and Wang, L. Highly reproducible surface-enhanced Raman spectra on semiconductor SnO<sub>2</sub> octahedral nanoparticles. *Spectrochimica Acta Part A: Molecular and Biomolecular Spectroscopy* (2012), 97, 1–6. <https://doi.org/10.1016/j.saa.2012.07.027>
- [29] Chen, X., Zhang, Z., & Lee, S. W. (2008). Selective solution-phase synthesis of BiOCl, BiVO<sub>4</sub>, and δ-Bi<sub>2</sub>O<sub>3</sub> nanocrystals in the reaction system of BiCl<sub>3</sub>–NH<sub>4</sub>VO<sub>3</sub>–NaOH. *Journal of Solid State Chemistry*, 181(1), 166–174. <https://doi.org/10.1016/j.jssc.2007.10.031>.
- [30] Sood, S., Zheng, G., & Gouma, P. (2014). High throughput synthesis of ceramic nanofibers. *MRS Online Proceedings Library*, 1659, 175–180. DOI: 10.1557/opl.2014.292
- [31] Nakamoto, K. (2009). *Infrared and Raman spectra of inorganic and coordination compounds* (6th ed.). John Wiley & Sons.

- [32] Dai, F., Zhuang, Q., Huang, G., Deng, H., Zhang, X., & Zhang, X. (2023). Infrared spectrum characteristics and quantification of OH groups in coal. *ACS Omega*, 8(17), 17064–17076. <https://doi.org/10.1021/acsomega.3c01336>
- [33] S. Kaur, A.S. Rao, M. Jayasimhadri, B. Sivaiah, D. Haranath, Synthesis optimization, photoluminescence and thermoluminescence studies of Eu<sup>3+</sup>-doped calcium aluminozincate phosphor, *J. Alloys Compd.* 802 (2019) 129–138, <https://doi.org/10.1016/j.jallcom.2019.06.169>.
- [34] N. Kaczorowska, A. Szczeszak, S. Lis, Synthesis and tunable emission studies of new up-converting Ba<sub>2</sub>GdV<sub>3</sub>O<sub>11</sub> nanopowders doped with Yb<sup>3+</sup>/Ln<sup>3+</sup> (Ln<sup>3+</sup>=Er<sup>3+</sup>, Ho<sup>3+</sup>, Tm<sup>3+</sup>), *J. Lumin.* 200 (2018) 59–65, <https://doi.org/10.1016/j.jlumin.2018.03.085>.
- [35] Pradip Z. Zambare, K. D. Girase, K. V. R. Murthy, O. H. Mahajan, Thermal analysis and luminescent properties of Sr<sub>2</sub>CeO<sub>4</sub> blue phosphor, *Adv. Mat. Lett.* 4(7) 2013, 577–581, <http://dx.doi.org/10.5185/amlett.2012.11457>.
- [36] Amit K. Vishwakarma, Kaushal Jha, M. Jayasimhadri, A.S. Rao, Kiwan Jang, B. Sivaiah, D. Haranath, *J. Alloys Comp.* 622 (2015), 97–101, <http://dx.doi.org/10.1016/j.jallcom.2014.10.016>.
- [37] U. Rambabu, N.R. Munirathnam, T.L. Prakash, S. Buddhudu, Emission spectra of LnPO<sub>4</sub>:RE<sup>3+</sup> (Ln = La, Gd; RE = Eu, Tb and Ce) powder phosphors, *Mater. Chem. Phys.* 78 (2002), 160–169, [https://doi.org/10.1016/S0254-0584\(02\)00294-8](https://doi.org/10.1016/S0254-0584(02)00294-8).
- [38] K. Maheshwari, A.S. Rao, Down-shifting photoluminescent properties of Tb<sup>3+</sup>-doped phosphate glasses for intense green-emitting devices applications, *Opt. Mater.* 137 (2023), 113533, <https://doi.org/10.1016/j.optmat.2023.113533> (Amst).
- [39] Sheetal Kumari, A.S. Rao, R.K. Sinha, Structural and photoluminescence properties of Sm<sup>3+</sup>-ions doped strontium yttrium tungstate phosphors for reddish-orange photonic device applications, *Mater. Res. Bull.* 167 (2023), 112419, <https://doi.org/10.1016/j.materresbull.2023.112419>.
- [40] G. Zhu, Z. Li, F. Zhou, C. Wang, S. Xin, A novel temperature sensitive Sm<sup>3+</sup>-doped niobate orange-red phosphor: The synthesis and characteristic luminescent property investigation, *J. Lumin.* 196 (2018) 32–35, <https://doi.org/10.1016/j.jlumin.2017.12.014>.
- [41] Q. Li, S. Zhang, W. Lin, W. Li, Y. Li, Z. Mu, F. Wu, A warmwhite emission of Bi<sup>3+</sup>-Eu<sup>3+</sup> and Bi<sup>3+</sup>-Sm<sup>3+</sup> codoping Lu<sub>2</sub>Ge<sub>2</sub>O<sub>7</sub> phosphors by energy transfer of Bi<sup>3+</sup>-sensitized Eu<sup>3+</sup>/Sm<sup>3+</sup>, *Spectrochim. Acta Part A Mol. Biomol. Spectrosc.* (2019), 117755 <https://doi.org/10.1016/j.saa.2019.117755>.


- [42] L. Wu, Y. Bai, L. Wu, H. Yi, Y. Kong, Y. Zhang, J. Xu, Sm<sup>3+</sup> and Eu<sup>3+</sup> codoped SrBi<sub>2</sub>B<sub>2</sub>O<sub>7</sub>: a red-emitting phosphor with improved thermal stability, *RSC Adv.* 7 (2017) 1146–1153, <https://doi.org/10.1039/c6ra26752a>.
- [43] X. Zhang, Z. Zhu, Z. Guo, Z. Sun, L. Zhou, Z. chao Wu, Synthesis, structure and luminescent properties of Eu<sup>3+</sup> doped Ca<sub>3</sub>LiMgV<sub>3</sub>O<sub>12</sub> color-tunable phosphor, *Ceram. Int.* 44 (2018) 16514–16521, <https://doi.org/10.1016/j.ceramint.2018.06.069>.
- [44] Sheetal Kumari, Pooja Rohilla, Aman Prasad, A.S. Rao, R.K. Sinha, Structural characterization and luminescence characteristics of Dy<sup>3+</sup> doped Sr<sub>9</sub>Y<sub>2</sub>W<sub>4</sub>O<sub>24</sub> phosphor for application in white-LEDs, *J. Lumin.* 275 (2024), 120791, <https://doi.org/10.1016/j.jlumin.2024.120791>.
- [45] I. Kumar, A. Kumar, S. Kumar, H. Thakur, A. K. Gathania, Synthesis, structure, and photoluminescence analysis of thermally stable Sm<sup>3+</sup> doped YPO<sub>4</sub> phosphor, *J. Phys. Conf. Ser.* 2663 (2023) 2–7, <https://doi.org/10.1088/1742-6596/2663/1/012002>.
- [46] Q. Long, C. Wang, Y. Li, J. Ding, X. Wang, Y. Wang, Solid state reaction synthesis and photoluminescence properties of Dy<sup>3+</sup> doped Ca<sub>3</sub>Sc<sub>2</sub>Si<sub>3</sub>O<sub>12</sub> phosphor, *Mater. Res. Bull.* 71 (2015) 21–24, <https://doi.org/10.1016/j.materresbull.2015.07.001>.
- [47] D. Xu, Synthesis and luminescence properties of double-perovskite white emitting phosphor Ca<sub>3</sub>WO<sub>6</sub>:Dy<sup>3+</sup>, *J. Mater. Sci. Mater. Electron.* (2016), <https://doi.org/10.1007/s10854-016-4848-z>.
- [48] B. Devakumar, H. Guo, Y. Zeng, X. Huang, Dyes and Pigments A single-phased warm-white-emitting K<sub>3</sub>Y(PO<sub>4</sub>)<sub>2</sub>:Dy<sup>3+</sup>, Sm<sup>3+</sup> phosphor with tuneable photoluminescence for near-UV-excited white LEDs, *Dyes Pigments* 157 (2018) 72–79, <https://doi.org/10.1016/j.dyepig.2018.04.042>.
- [49] Sheetal Kumari, Pooja Rohilla, Samarthya Diwakar, Rupesh A. Talewar, Ankur Shandilya, Yasha Tayal, K. Swapna, Aman Prasad, and A. S. Rao, Synthesis, analysis and characterizations of Dy<sup>3+</sup> ions-doped CaBi<sub>2</sub>Nb<sub>2</sub>O<sub>9</sub> phosphors for optoelectronic device applications, *J Mater Sci: Mater Electron* (2024) 35:867, <https://doi.org/10.1007/s10854-024-12640-2>.
- [50] Sheetal Kumari, A.S. Rao, R.K. Sinha, Investigations on photoluminescence and energy transfer studies of Sm<sup>3+</sup> and Eu<sup>3+</sup> ions doped Sr<sub>9</sub>Y<sub>2</sub>W<sub>4</sub>O<sub>24</sub> red emitting phosphors with high color purity for w-LEDs, *J. Mol. Struct.* 1295 (2024), 136507, <https://doi.org/10.1016/j.molstruc.2023.136507>.



- [51] V. Chauhan, P. Deshmukh, S. Satapathy, P.C. Pandey, Results in physics greenish- yellow emission from rare-earth free Li+doped zinc vanadate phosphor, Results Phys 39 (2022), 105689, <https://doi.org/10.1016/j.rinp.2022.105689>.
- [52] V. Uma, M. Vijayakumar, K. Marimuthu, G. Muralidharan, Luminescence and energy transfer studies on Sm<sup>3+</sup>/Tb<sup>3+</sup>+codoped telluroborate glasses for WLED applications, J. Mol. Struct. 1151 (2018) 266–276, <https://doi.org/10.1016/j.molstruc.2017.09.053>.
- [53] M. Yan, G. Liu, J. Wen, Y. Wang, Blue-light-excited Eu<sup>3+</sup>/Sm<sup>3+</sup>+Co-doped NaLa (MoO<sub>4</sub>)<sub>2</sub> phosphors: synthesis, characterizations and red emission enhancement for WLEDs, Materials (Basel) 11 (2018), <https://doi.org/10.3390/ma11071090>.
- [54] P. Dang, D. Liu, Y. Wei, G. Li, H. Lian, M. Shang, J. Lin, Highly efficient cyan-green emission in self-activated Rb<sub>3</sub>RV<sub>2</sub>O<sub>8</sub> (R =Y, Lu) vanadate phosphors for full- spectrum white light-emitting diodes (LEDs), Inorg. Chem. 59 (2020) 6026–6038, <https://doi.org/10.1021/acs.inorgchem.0c00015>.
- [55] R. Lohan, A. Kumar, M.K. Sahu, A. Mor, V. Kumar, N. Deopa, A.S. Rao, Structural, thermal, and luminescence kinetics of Sr<sub>4</sub>Nb<sub>2</sub>O<sub>9</sub> phosphor doped with Dy<sup>3+</sup>ions for cool w-LED applications, J. Mater. Sci. Mater. Electron. 34 (2023) 1–21, <https://doi.org/10.1007/s10854-023-10055-z>.
- [56] A.S.Rao Ravita, Tunable photoluminescence studies of KZABS: RE<sup>3+</sup>+(RE<sup>3+</sup>=Tm<sup>3+</sup>, Tb<sup>3+</sup>and Sm<sup>3+</sup>) glasses for w-LEDs based on energy transfer, J. Lumin. 251 (2022), <https://doi.org/10.1016/j.jlumin.2022.119194>.

# PLAGIARISM REPORT

## Thesis Draft (For Plag-Check).pdf

 Delhi Technological University

### Document Details

Submission ID tnm-oid:-27535-99690102	21 Pages
Submission Date Jun 6, 2025, 9:26 PM GMT+5:30	7,961 Words
Download Date Jun 6, 2025, 9:30 PM GMT+5:30	44,742 Characters
File Name Thesis Draft (For Plag-Check).pdf	
File Size 324.8 KB	



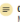

## 7% Overall Similarity

The combined total of all matches, including overlapping sources, for each database.




### Filtered from the Report

- Bibliography
- Small Matches (less than 12 words)

### Match Groups

-  **34 Not Cited or Quoted 6%**  
Matches with neither in-text citation nor quotation marks
-  **1 Missing Quotations 0%**  
Matches that are still very similar to source material
-  **0 Missing Citation 0%**  
Matches that have quotation marks, but no in-text citation
-  **0 Cited and Quoted 0%**  
Matches with in-text citation present, but no quotation marks

### Top Sources

-  **3%** Internet sources
-  **3%** Publications
-  **4%** Submitted works (Student Papers)


### Integrity Flags

#### 0 Integrity Flags for Review

No suspicious text manipulations found.

Our system's algorithms look deeply at a document for any inconsistencies that would set it apart from a normal submission. If we notice something strange, we flag it for you to review.

A flag is not necessarily an indicator of a problem. However, we'd recommend you focus your attention there for further review.

Page 3 of 26 - Integrity Overview

Submission ID tm oid: 27535-99690102

Match Groups

34 Not Cited or Quoted 6%

Matches with neither in-text citation nor quotation marks

1 Missing Quotations 0%

Matches that are still very similar to source material

0 Missing Citation 0%

Matches that have quotation marks, but no in-text citation

0 Cited and Quoted 0%

Matches with in-text citation present, but no quotation marks

Top Sources

3% Internet sources

3% Publications

4% Submitted works (Student Papers)

Top Sources

The sources with the highest number of matches within the submission. Overlapping sources will not be displayed.

1 Publication

Pooja Rohilla, A. S. Rao. "Energy transfer induced colour tunable photoluminesce...

<1%

2 Internet

www.researchgate.net

<1%

3 Submitted works

Khalifa University of Science Technology and Research on 2024-12-05

<1%

4 Internet

research.mrl.ucsb.edu

<1%

5 Internet

www.intechopen.com

<1%

6 Publication

S. Murugan, G. Vignesh, M. Ashok kumar. "Investigating the Influence of CuS Rati...

<1%

7 Submitted works

University of Surrey on 2024-08-29

<1%

8 Submitted works

University of Sheffield on 2025-03-27

<1%

9 Submitted works


Hong Kong University of Science and Technology on 2023-03-09

<1%


10 Submitted works

UCL on 2025-05-06

<1%

Page 3 of 26 - Integrity Overview

Submission ID tm oid: 27535-99690102

Page 4 of 26 - Integrity Overview

Submission ID tm oid: 27535-99690102

11 Internet

www.photonics.com

<1%

12 Publication

Guorui Yang, Wei Yan, Qian Zhang, Shaohua Shen, Shujiang Ding. "One-dimensio...

<1%

13 Internet

ijarjie.com

<1%

14 Submitted works

Higher Education Commission Pakistan on 2018-12-04

<1%

15 Publication

Jiaqi Long, Fujuan Chu, Yuzhen Wang, Chong Zhao et al. " M Mg5c(PO ) : Dy (M ...

<1%

16 Submitted works

Middlesex University on 2025-04-13

<1%

17 Publication

Sarah Kate Wilson, Milica Stojanovic, Muriel Medard, Kurt Schab. "Random Guessi...

<1%

18 Publication

Jing Zhang, Ge-Mei Cai, Lv-Wei Yang, Zhi-Yuan Ma, Zhan-Peng Jin. " Layered Cryst...

<1%

19 Submitted works

National University of Singapore on 2012-11-19

<1%

20 Submitted works

Universiti Teknologi Malaysia on 2014-08-21

<1%

21 Internet

pure.unileoben.ac.at

<1%

22 Submitted works

City University of Hong Kong on 2023-11-15

<1%

23 Submitted works

IIT Delhi on 2023-06-13

<1%

24 Publication

Mihail Nazarov, Do Young Noh. "New Generation of Europium- and Terbium-Activ...

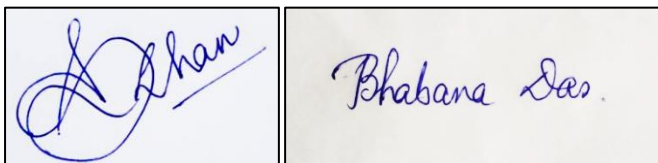
<1%

Page 4 of 26 - Integrity Overview

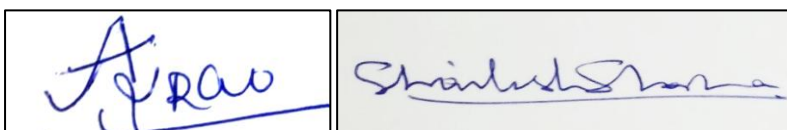
Submission ID tm oid: 27535-99690102

25	Submitted works	North-Eastern Hill University, Shillong on 2024-01-18	<1%
26	Submitted works	Visvesvaraya National Institute of Technology on 2022-09-12	<1%
27	Internet	docksci.com	<1%
28	Internet	resumecat.com	<1%
29	Internet	tel.archives-ouvertes.fr	<1%
30	Internet	www.mdpi.com	<1%

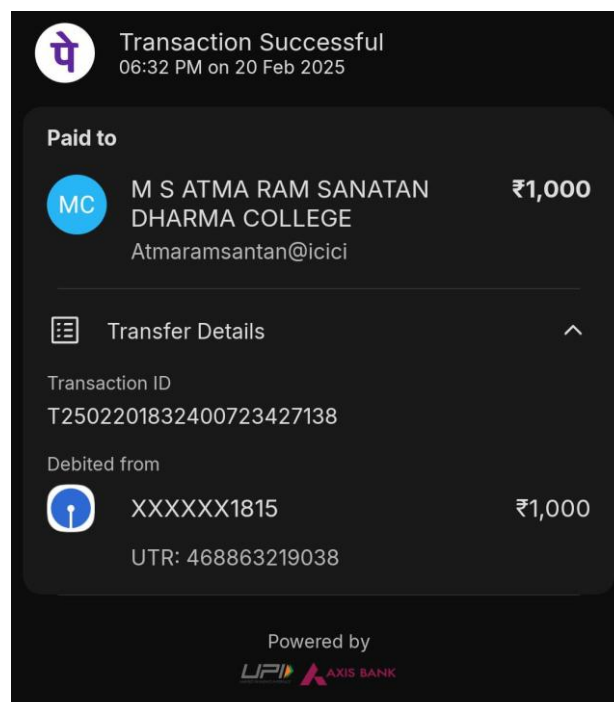
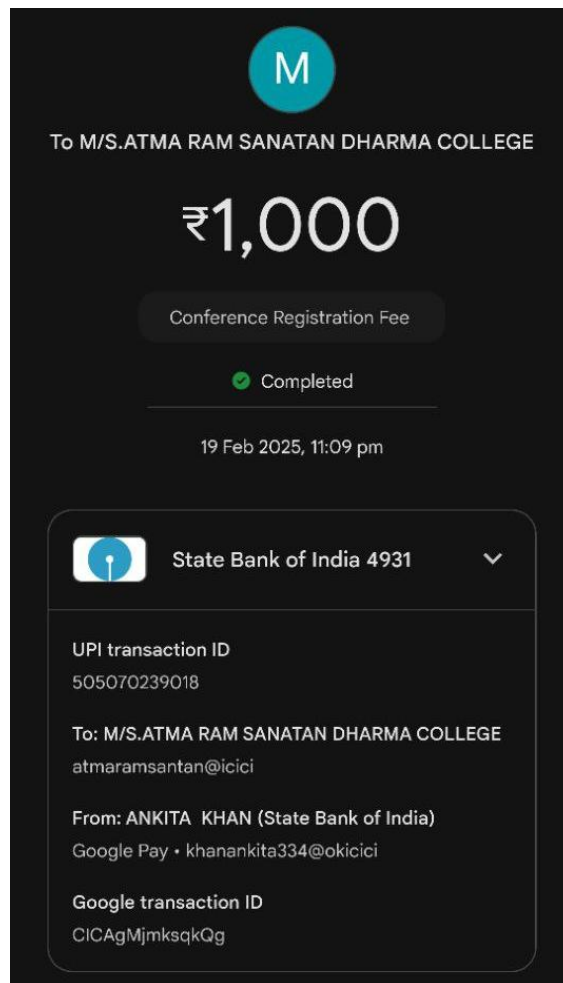
**Students' signatures: Ankita Khan & Bhabana Das**



**Supervisors' signatures: Prof. A.S. Rao & Prof. Shailesh Narain Sharma**



## REGISTRATION AND PAYMENT PROOFS





# Acceptance Letter for 3rd International Conference on Advanced Functional Materials & Devices for Sustainable Development (AFMD-2025) at ARSD College

afmd2025@arsd.du.ac.in  
To: kharankita334@gmail.com

Mon, 17 Feb, 2025 at 7:05 pm

## Acceptance Letter – AFMD-2025

Dear Prof./Dr./Mr./Ms. ANKITA KHAN  
DELHI TECHNOLOGICAL UNIVERSITY

Greetings from the organizing committee of the International Conference on "Advanced Functional Materials & Devices for Sustainable Development (AFMD-2025)." The conference will be held in hybrid mode\* (online & offline) at Atma Ram Sanatan Dharma College, University of Delhi, from March 03-05, 2025. It is being organized by the Department of Physics and Internal Quality Assurance cell (IQAC) of ARSD College.

We are pleased to inform you that the technical committee has accepted your participation, titled:

**PP-96: Synthesis, Morphology and Luminescent Properties of  $\text{Ca}_3\text{Y}_2\text{WO}_9\text{:Dy}^{3+}$  Phosphors for w-LED applications**

**Type of Presentation: Poster Presentation-Online via Google Meet/Zoom**

**\*Program will take place as per following manner:**

- Day-1 Offline Mode at ARSD College
- Day 2&3 Online Mode through Zoom or Google Meet

Kindly confirm your participation by submitting the registration fee in favor of Atma Ram Sanatan Dharma College using the following bank details:

- Bank Name: ICICI Bank
- A/c No: 017101020425
- IFSC: ICIC0000171
- Branch: Saket, New Delhi
- SWIFT Code: ICICINBBNRI

Dear Participants  
Greetings!!!  
You are requested to fill correct details in this form same will be published on your certificate

Category	Registration before 20th Feb 2025		After 20th Feb 2025	
	Indian (INR)	Foreign (USD)	Indian (INR)	Foreign (USD)
Students	1000	75	1500	100
Faculty/Scientist /Researcher	2000	100	3000	150

**\*Fee is non refundable**

**Bank Details**

- Payment must be made online through Net banking/NEFT
- Name: Atma Ram Sanatan Dharma College
- Bank Name: ICICI Bank
- A/c No. 017101020425
- IFSC: ICIC0000171
- Branch: Saket, New Delhi
- SWIFT Code: ICICINBBNRI

Scan QR code & Pay  
UPI/BHIM/PayTM/Phonepe

## Development (AFMD-2025) at ARSD College



afmd2025@arsd.d... Feb 16

to me

## Acceptance Letter – AFMD-2025

Dear Prof./Dr./Mr./Ms. BHABANA DAS  
DELHI TECHNOLOGICAL UNIVERSITY

Greetings from the organizing committee of the International Conference on "Advanced Functional Materials & Devices for Sustainable Development (AFMD-2025)." The conference will be held in hybrid mode\* (online & offline) at Atma Ram Sanatan Dharma College, University of Delhi, from March 03-05, 2025. It is being organized by the Department of Physics and Internal Quality Assurance cell (IQAC) of ARSD College.

We are pleased to inform you that the technical committee has accepted your participation, titled:

**PP-83: Synthesis, Morphology and Luminescent Properties of  $\text{Ca}_3\text{Y}_2\text{WO}_9\text{:Dy}^{3+}$  Phosphors for w-LED applications**

**Type of Presentation: Poster Presentation-Online via Google Meet/Zoom**

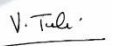

**\*Program will take place as per following manner:**

## CONFERENCE PARTICIPATION CERTIFICATES




**ATMA RAM SANATAN DHARMA COLLEGE**  
**UNIVERSITY OF DELHI**  
Accredited Grade 'A++' By NAAC || All India 5th Rank in NIRF (Ministry of Education)  
3rd International Conference on  
**Advanced Functional Materials and Devices (AFMD-2025)**  
for Sustainable Development  
Under the aegis of IQAC and supported by Department of Biotechnology (GoI)

*Certificate of Participation*  
This is to certify that Prof./Dr./Mr./Ms.  
**ANKITA KHAN**  
**DELHI TECHNOLOGICAL UNIVERSITY**  
has participated in the 3rd International Conference on "Advanced Functional Materials & Devices for Sustainable Development" (AFMD-2025) organised by Department of Physics under the aegis of IQAC ARSD College, University of Delhi, India during March 03-05, 2025 in hybrid mode.  
He/She has presented **Poster** entitled:  
**PP-79:-Synthesis, Morphology and Luminescent Properties of Ca<sub>3</sub>Y<sub>2</sub>WO<sub>9</sub>:Dy<sup>3+</sup> Phosphors for w-LED applications**

  
**Dr. Shankar Subramanian**  
Convener, AFMD-2025  
**Dr. Anjali Sharma**  
Convener, AFMD-2025  
**Prof. Vinita Tuli**  
Coordinator, IQAC  
**Prof. Gyantosh Kumar Jha**  
Principal/Patron AFMD-2025

Certificate No: ARSD/AFMD25/PP/082



**ATMA RAM SANATAN DHARMA COLLEGE**  
**UNIVERSITY OF DELHI**  
Accredited Grade 'A++' By NAAC || All India 5th Rank in NIRF (Ministry of Education)  
3rd International Conference on  
**Advanced Functional Materials and Devices (AFMD-2025)**  
for Sustainable Development  
Under the aegis of IQAC and supported by Department of Biotechnology (GoI)

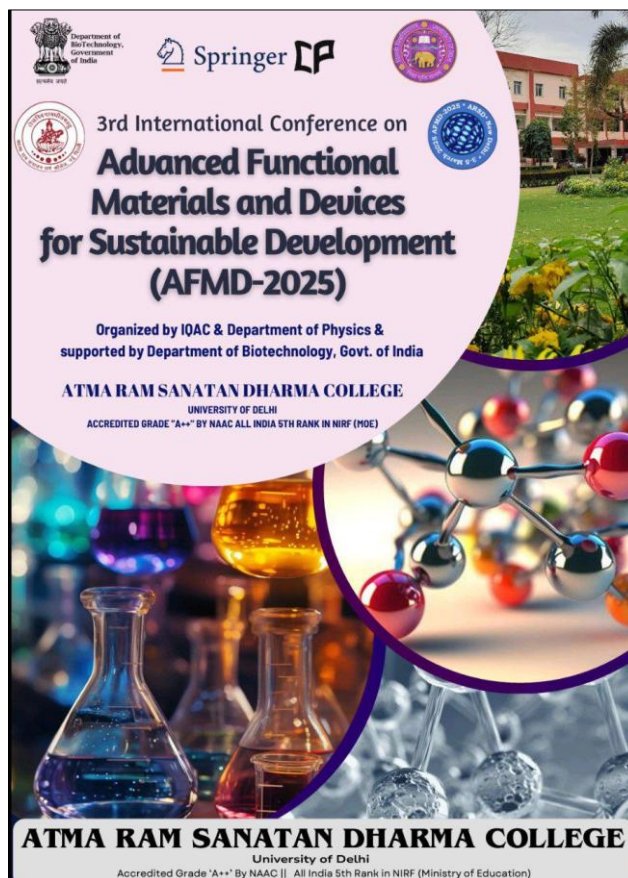
*Certificate of Participation*  
This is to certify that Prof./Dr./Mr./Ms.  
**BHABANA DAS**  
**DELHI TECHNOLOGICAL UNIVERSITY**  
has participated in the 3rd International Conference on "Advanced Functional Materials & Devices for Sustainable Development" (AFMD-2025) organised by Department of Physics under the aegis of IQAC ARSD College, University of Delhi, India during March 03-05, 2025 in hybrid mode.  
He/She has presented **Poster** entitled:  
**PP-83:-Synthesis, Morphology and Luminescent Properties of Ca<sub>3</sub>Y<sub>2</sub>WO<sub>9</sub>:Dy<sup>3+</sup> Phosphors for w-LED applications**

  
**Dr. Shankar Subramanian**  
Convener, AFMD-2025  
**Dr. Anjali Sharma**  
Convener, AFMD-2025  
**Prof. Vinita Tuli**  
Coordinator, IQAC  
**Prof. Gyantosh Kumar Jha**  
Principal/Patron AFMD-2025

Certificate No: ARSD/AFMD25/PP/087



## CONFERENCE BOOK OF ABSTRACTS ACCEPTANCE PROOF



PP-79

### Synthesis, Morphology and Luminescent Properties of $\text{Ca}_3\text{Y}_2\text{WO}_9:\text{Dy}^{3+}$ Phosphors for w-LED applications

Ankita Khan, Bhabana Das, A. S. Rao\*

*Department of Applied Physics, Delhi Technological University, Shahbad Daulatpur, Main Bawana Road, Delhi-110042, India*

\*[drsallam@gmail.com](mailto:drsallam@gmail.com)

#### ABSTRACT

$\text{Dy}^{3+}$  ions doped Calcium Yttrium Tungstate ( $\text{Ca}_3\text{Y}_2\text{WO}_9$ ) ( $\text{CaYW}$ ) phosphors were synthesized via the conventional solid-state reaction method. The undoped and doped phosphor samples were characterized by X-ray diffraction (XRD) method, and the diffraction peaks of the sample sintered at  $1100^\circ\text{C}$  closely resembled those of the standard JCPDS pattern with card number 00-038-0218, and the crystal system was found to be tetragonal. The optical bandgap value was measured using diffuse reflectance spectra (DRS). A series of  $\text{CaYW}:\text{x}\text{Dy}^{3+}$  phosphors with different doping concentrations of  $\text{Dy}^{3+}$  ( $\text{x}=1\text{ mol}\%$ ,  $3\text{ mol}\%$ ,  $5\text{ mol}\%$ ,  $7\text{ mol}\%$ ,  $9\text{ mol}\%$ ,  $11\text{ mol}\%$ ) were synthesized, and their photoluminescence spectra (PL) were studied. The PL emission spectra revealed that the phosphors, when excited at  $352\text{ nm}$ , showed emission at  $575\text{ nm}$  corresponding to the transition  $^4\text{F}_{3/2} \rightarrow ^6\text{H}_{15/2}$ , and concentration quenching occurred after  $9\text{ mol}\%$  of  $\text{Dy}^{3+}$  ions. Therefore, the optimum concentration for the phosphor is  $9\text{ mol}\%$  of  $\text{Dy}^{3+}$  ions. The CIE chromaticity coordinates were estimated for all the phosphor samples and were found to be in the white region, and the chromaticity coordinates for the optimized sample was evaluated to be  $(0.365, 0.397)$ . In conclusion, the results of the current study demonstrate that  $\text{Dy}^{3+}$  ions doped  $\text{CaYW}$  phosphors may have applications in w-LEDs.

**Keywords:** doping; phosphor; photoluminescence; w-LEDs.



## SUBMISSION TO JOURNAL OF ELECTRONIC MATERIALS

JEMS-D-25-01000 - Submission  
Notification to co-author -  
[EMID:c1066066cec34f37] Inbox



Journal of Elec... 30 Apr

to me ▾



Re:

Submission ID: JEMS-D-25-01000

"Synthesis, morphology and luminescent properties of  $\text{Ca}_3\text{Y}_2\text{WO}_9:\text{Dy}^{3+}$  phosphors for w-LED applications"

Full author list: Ankita Khan; Bhabana Das; Bhawna Rajpal; Aarti Yadav; Shailesh Narain Sharma; A.S. Rao

Dear Ms. Khan,

We have received the submission entitled: "Synthesis, morphology and luminescent properties of  $\text{Ca}_3\text{Y}_2\text{WO}_9:\text{Dy}^{3+}$  phosphors for w-LED applications" for possible publication in Journal of Electronic Materials, and you are listed as one of the co-authors.

The manuscript has been submitted to the journal by Dr. Dr. Shailesh Sharma who will be able to track the status of the paper through his/her login.

If you have any objections, please contact the editorial office as soon as possible. If we do not hear back from you, we will assume you agree with your co-authorship.

Thank you very much.

With kind regards,

Springer Journals Editorial Office  
Journal of Electronic Materials

# PROOF OF SCIE/SCOPUS INDEX

Filters [Clear All](#)

Web of Science Coverage ^

**Core Collection**

- ☒ Science Citation Index Expanded (SCIE)
- ☐ Social Sciences Citation Index (SSCI)
- ☐ Arts & Humanities Citation Index (AHCI)
- ☐ Emerging Sources Citation Index (ESCI)

**Current Contents**

- ☐ Agriculture, Biology & Environmental Sciences
- ☐ Arts & Humanities

SCIENCE CITATION INDEX EXPANDED (SCIE) x

Search Results

Found 1,050 results (Page 1) [Share These Results](#)

Exact Match Found

**JOURNAL OF ELECTRONIC MATERIALS**

Publisher: **SPRINGER** ONE NEW YORK PLAZA, SUITE 4600 , NEW YORK, United States, NY, 10004

ISSN / eISSN: 0361-5235 / 1543-186X

Web of Science Core Collection: **Science Citation Index Expanded**

Additional Web of Science Indexes: Current Contents Electronics & Telecommunications Collection | Current Contents Physical, Chemical & Earth Sciences | Essential Science Indicators

[Share This Journal](#) [View profile page](#)

**Journal information**

Electronic ISSN	Print ISSN
1543-186X	0361-5235

**Abstracted and indexed in**

- Astrophysics Data System (ADS)
- BFI List
- Baidu
- CLOCKSS
- CNKI
- CNPIEC
- Chemical Abstracts Service (CAS)
- Chimica
- Current Contents/Electronics & Telecommunications Collection
- Current Contents/Physical, Chemical and Earth Sciences
- Dimensions
- EBSCO
- El Compendex
- Google Scholar
- INSPEC
- Japanese Science and Technology Agency (JST)
- Naver
- OCLC WorldCat Discovery Service
- Portico
- ProQuest
- SCImago
- SCOPUS**
- Science Citation Index Expanded (SCIE)**
- Semantic Scholar
- TD Net Discovery Service
- Wanfang

<https://link.springer.com/journal/11664>